UNIVERSITY OF OKLAHOMA

GRADUATE COLLEGE

INVESTIGATION OF ANTENNA EDGE TREATMENTS AND GROUND PLANE COUPLING BEHAVIOR

A THESIS

SUBMITTED TO THE GRADUATE FACULTY

in partial fulfillment of the requirements for the

Degree of

MASTER OF SCIENCE

By

ANDRIUS VYTENIS LIETUVNINKAS

Norman, Oklahoma

2016

Downloaded from SHAREOK. Persistent Handle URL: https://hdl.handle.net/11244/47075

INVESTIGATION OF ANTENNA EDGE TREATMENTS AND GROUND PLANE COUPLING BEHAVIOR

A THESIS APPROVED FOR THE
SCHOOL OF ELECTRICAL AND COMPUTER ENGINEERING

BY

Dr. Jessica Ruyle, Chair

Dr. Caleb Fulton

Dr. Hjalti Sigmarsson

© Copyright by ANDRIUS VYTENIS LIETUVNINKAS 2016
All Rights Reserved.

Table of Contents

List of Tables **vi**

List of Figures **vii**

Abstract **xiii**

1 Introduction **1**
1.1 Motivation 1
1.2 Thesis Outline 7

2 Edge Treatment Variation Investigation **8**
2.1 Introduction 8
2.2 Comparison of Different Structures 11
2.3 Performance Analysis 13
2.4 Radiation Patterns 19
2.5 VSWR and Power Radiated - Additional Cases 28
2.6 Conclusions 30

3 Side Study on Disconnected Apertures **32**
3.1 Introduction 32
3.2 Changing Disconnected Arm Length 33
3.3 Isolated Aperture Arms 39
3.4 Transmission Line Model of Aperture Discontinuity 41
3.5 Conclusions 44

4 Application to Large Ground Plane **46**
4.1 Introduction 46
4.2 Edge Treatments on Ground Plane 47
4.3 Antenna Design 51
4.4 Simulated Antenna Performance Off and On Large Ground Plane . . 54
4.5 Conclusions 59

5 Measurements **61**
5.1 Introduction 61
5.2 Constructed Entities 62
5.3 Characteristic Mode Analysis 67
5.4 Measured Results 69
5.5 Conclusions 85

6 Conclusions/Future Work **86**
6.1 Conclusions 86
6.2 Future Work 88

References **89**

List of Tables

2.1 VSWR minima observed for each edge treatment for the electrically small case. 15

3.1 Table of disconnected aperture structure dimensions used in HFSS simulation. All dimension are in millimeters. 43

4.1 Key dimensions of antenna from Figure 4.4. 52

4.2 Radiation efficiencies and peak realized gain for each edge treatment's operating electrical size on the antenna. Data is obtained from HFSS for each antenna with truncated conductor backing and extended ground plane backing. No data was obtained of the antenna with triangular apertures edge treatment. GP stands for ground plane. 58

5.1 Measured and simulated broadside realized gain for each antenna when containing truncated conductor backing and when placed on larger ground plane. Data shown for co-pol (θ) patterns. 84

5.2 Measured and simulated broadside realized gain for each antenna when containing truncated conductor backing and when placed on larger ground plane. Data shown for cross pol (ϕ) patterns. 84

List of Figures

1.1 (Top) Placement insensitive antenna; (Bottom) Slot fields coupling into parallel plate waveguide. 2
1.2 (a) Phi polarization of realized gain of placement insensitive antenna in the $\phi = 0$ cut plane when not containing backing ground plane (b) Theta and phi polarizations of realized gain of placement insensitive antenna in the $\phi = 0$ cut plane when containing backing ground plane.[1] 4

2.1 (a): Parallel plate waveguide with serrated edge, (b): VSWR of serrated parallel plate waveguide with various serration depth electrical sizes. 9
2.2 Placement insensitive antenna that different edge treatments are being studied for [1]. 10
2.3 (a)Left to right: triangular serration, half-circle serration, curved serration, subtriangular serration. (b)Left to right: triangular aperture, circular aperture, diamond aperture. 11
2.4 Parallel plate structure under consideration. Serrated edges are base model used for comparison. 12
2.5 VSWR of each structure at $w = 40mm$ and $d = 30mm$. The abscissa is the depth of the edge treatment normalized to free space wavelength. Apertures are at dimensions $0.875d$, $0.667d$, and $0.5303d$ respectively in the order as shown in legend 14
2.6 Vector electric fields plotted on the HFSS model for the structure containing triangular aperture edge treatments which show the existence of a higher order mode on the structure. 16
2.7 Vector electric fields plotted on the HFSS model for the structure containing subtriangular edge treatments which show the existence of a higher order mode on the structure. 16
2.8 Peak realized gain in dB of each structure from Figure 2.5. 18
2.9 Total power radiated in dBm of each structure from Figure 2.5. . . . 19
2.10 Realized Gain of triangular serrations across Θ for both polarizations. Θ-polarization is represented by the solid lines and Φ-polarization is represented by the dashed lines. 20

2.11 Realized Gain of triangular serrations across Φ for both polarizatoins. Θ-polarization is represented by the solid lines and Φ-polarization is represented by the dashed lines. 20
2.12 Realized Gain of half-circles across Θ for both polarizations. Θ-polarization is represented by the solid lines and Φ-polarization is represented by the dashed lines. 21
2.13 Realized Gain of half-circles across Φ for both polarizatoins. Θ-polarization is represented by the solid lines and Φ-polarization is represented by the dashed lines. 21
2.14 Realized Gain of curved serrations across Θ for both polarizations. Θ-polarization is represented by the solid lines and Φ-polarization is represented by the dashed lines. 22
2.15 Realized Gain of curved serrations across Φ for both polarizatoins. Θ-polarization is represented by the solid lines and Φ-polarization is represented by the dashed lines. 22
2.16 Realized Gain of subtriangular serrations across Θ for both polarizations. Θ-polarization is represented by the solid lines and Φ-polarization is represented by the dashed lines. 23
2.17 Realized Gain of subtriangular serrations across Φ for both polarizatoins. Θ-polarization is represented by the solid lines and Φ-polarization is represented by the dashed lines. 23
2.18 Realized Gain of triangular serrations with triangular apertures across Θ for both polarizations. Θ-polarization is represented by the solid lines and Φ-polarization is represented by the dashed lines. 24
2.19 Realized Gain of triangular serrations with triangular apertures across Φ for both polarizatoins. Θ-polarization is represented by the solid lines and Φ-polarization is represented by the dashed lines. 24
2.20 Realized Gain of triangular serrations with diamond apertures across Θ for both polarizations. Θ-polarization is represented by the solid lines and Φ-polarization is represented by the dashed lines. 25
2.21 Realized Gain of triangular serrations with diamond apertures across Φ for both polarizatoins. Θ-polarization is represented by the solid lines and Φ-polarization is represented by the dashed lines. 25
2.22 Realized Gain of triangular serrations with circle apertures across Θ for both polarizations. Θ-polarization is represented by the solid lines and Φ-polarization is represented by the dashed lines. 26
2.23 Realized Gain of triangular serrations with circle apertures across Φ for both polarizatoins. Θ-polarization is represented by the solid lines and Φ-polarization is represented by the dashed lines. 26
2.24 VSWR and Power radiated in dBm for for different edge treatment dimensions with no apertures. Edge treatment width and depth are $w = 20mm$ and $d = 30mm$. 29

2.25 VSWR and Power radiated in dBm for only structures with apertures. Edge treatment width and depth are $w = 40mm$ and $d = 30mm$. Dashed lines represent triangular apertures, dash-dot lines represent circle apertures, and dashed lines represent diamond apertures. 30

3.1 HFSS model of the triangular apertures edge treatment structure with disconnected aperture. 33
3.2 VSWR of each structure across frequency. Each curve represents a different arm length. As arm length ncreases, dip in VSWR shifts down in frequency. 34
3.3 The frequencies at which the arm lengths experience impedance matches and their corresponding normalized electrical length. 35
3.4 Total power radiated of each structure across frequency. Each curve represents a different arm length. A spike corresponding to an increased power radiated is shown to correspond with each structures' respective dip in VSWR. 36
3.5 Realized gain theta polarization Θ-cut plane at $\Phi = 90°$. 37
3.6 Realized gain theta polarization Φ-cut plane at $\Theta = 90°$. 37
3.7 Realized gain phi polarization Φ-cut plane at $\Theta = 90°$. 38
3.8 Peak realized gain for each structure across frequency. Each curve represents a different arm length. 38
3.9 Aperture arm structures 40
3.10 3.10(a): VSWR when varying bend angle θ, and 3.10(b): VSWR when varying arm width w_a 41
3.11 Transmission-line model for the edge treatment structure containing apertures and the radiating arms. 42
3.12 Input impedance of transmission-line model for the edge treatment structure containing apertures and the radiating arms. The curves are designated as TL## or HFSS## in which the ## corresponds to a serration depth mentioned in Table 3.1. 44

4.1 (a): Currents induced on ground plane from the triangular serration edge treatment; (b) Currents induced on a ground plane from the triangular aperture edge treatment containing disconnected apertures on the ends. 48

4.2 Plots comparing the performance of the triangular serration edge treatments (blue curves) and the triangular aperture edge treatments (green curves) when radiating onto a ground plane vs into freespace where (a): VSWR; (b) power radiated in dBm; (c) peak realized gain in dB; (d) radiation efficiency. The freespace curves pertain to when the edge treatment is simulated with the truncated conductor backing, and the ground plane curves pertain to the extended ground plane case shown in Figure 4.1. 49
4.3 Antenna design GUI for conductor-backed spiral inductor loaded slot antenna containing serrated edges. 51
4.4 HFSS model for antenna containing triangular serrations given by the antenna design program. 53
4.5 HFSS models of each additional edge treatment structure included in the antenna. Left to right: ellipse, curved, subtriangular, triangular apertures. 54
4.6 Input impedance for each antenna containing a different edge treatment, with each curve named after which edge treatment the antenna contains. 55
4.7 Antenna containing triangular serration edge treatment next to its 3-dimensional realized gain pattern. 56
4.8 Antenna containing triangular serration edge treatment placed on larger ground plane. (Top left) Orientation of the slot on the ground plane; (Bottom left) Realized gain pattern for the antenna on the larger ground plane; (Right) Induced current magnitude on the ground plane with arrows indicating direction of current flow. 57

5.1 Fabricated conductor-backed slot antenna containing the triangular serration edge treatment. 63
5.2 Fabricated conductor-backed slot antenna containing the ellipse serration edge treatment. 63
5.3 Fabricated conductor-backed slot antenna containing the curved serration edge treatment. 64
5.4 Fabricated conductor-backed slot antenna containing the subtriangular serration edge treatment. 64
5.5 Fabricated conductor-backed slot antenna containing the triangular apertures serration edge treatment. 65
5.6 The conductor-backed antenna containing the triangular aperture serrations mounted in the anechoic chamber. Feed structure contains quarter-wave bazooka balun. 66
5.7 Calibration dipole at the operating frequency of the antenna containing the triangular serrations mounted in the anechoic chamber. . 67
5.8 The $8'x8'$ ground plane mounted in the anechoic chamber. 68

5.9 (a) Magnitude and (b) direction of mode 1 surface currents on ground plane at 440.5 MHz, which corresponds to operating frequency of antenna containing triangular serration edge treatments. Length and height designated as electrical size of ground plane at operating frequency. 70
5.10 (a) Magnitude and (b) direction of mode 1 surface currents on ground plane at 380.1 MHz, which corresponds to operating frequency of antenna containing ellipse serration edge treatments. Length and height designated as electrical size of ground plane at operating frequency. 70
5.11 (a) Magnitude and (b) direction of mode 1 surface currents on ground plane at 578.9 MHz, which corresponds to operating frequency of antenna containing curved serration edge treatments. Length and height designated as electrical size of ground plane at operating frequency. 71
5.12 (a) Magnitude and (b) direction of mode 1 surface currents on ground plane at 540.1 MHz, which corresponds to operating frequency of antenna containing subtriangle serration edge treatments. Length and height designated as electrical size of ground plane at operating frequency. 71
5.13 (a) Magnitude and (b) direction of mode 1 surface currents on ground plane at 450.9 MHz, which corresponds to operating frequency of antenna containing triangular aperture serration edge treatments. Length and height designated as electrical size of ground plane at operating frequency. 72
5.14 S_{11} measured vs simulated for the conductor-backed slot antenna containing the triangular serration edge treatment. 73
5.15 S_{11} measured vs simulated for the conductor-backed slot antenna containing the ellipse serration edge treatment. 74
5.16 S_{11} measured vs simulated for the conductor-backed slot antenna containing the curved serration edge treatment. 75
5.17 S_{11} measured vs simulated for the conductor-backed slot antenna containing the subtriangular serration edge treatment. 76
5.18 S_{11} measured vs simulated for the conductor-backed slot antenna containing the triangular aperture serration edge treatment. 77
5.19 Measured vs simulated (a) realized Gain θ and (b) realized gain ϕ of antenna containing the triangular serration edge treatment. Solid lines correspond to antenna pattern without ground plane, while dashed lines correspond to antenna pattern mounted on ground plane. 78

5.20 Measured vs simulated (a) realized Gain θ and (b) realized gain ϕ of antenna containing the ellipse serration edge treatment. Solid lines correspond to antenna pattern without ground plane, while dashed lines correspond to antenna pattern mounted on ground plane. . . . 79
5.21 Measured vs simulated (a) realized Gain θ and (b) realized gain ϕ of antenna containing the curved serration edge treatment. Solid lines correspond to antenna pattern without ground plane, while dashed lines correspond to antenna pattern mounted on ground plane. . . . 80
5.22 Measured vs simulated (a) realized Gain θ and (b) realized gain ϕ of antenna containing the subtriangular serration edge treatment. Solid lines correspond to antenna pattern without ground plane, while dashed lines correspond to antenna pattern mounted on ground plane. 81
5.23 Measured vs simulated (a) realized Gain θ and (b) realized gain ϕ of antenna containing the triangular aperture serration edge treatment. Solid lines correspond to antenna pattern without ground plane, while dashed lines correspond to antenna pattern mounted on ground plane. 82

Abstract

Guided wave structures can perform as broadband antenna elements through the use of a gradual impedance transformation. The impedance match is typically created through gradual structural changes to match the impedance of the guide to that of free space. For parallel plate waveguide, it has been shown that serrating the edge of one of the conductors at the truncation between the waveguide and freespace can minimize reflection at that plane and present a broad impedance match between the waveguide and freespace. This method, however, is most effective when the parallel plate and serration are an appreciable size of a wavelength. This work presents potential alternative edge treatment designs other than the triangular serration for better impedance matching and radiation performance, particularly at small electrical sizes. This study extends the insights gathered from the edge treatment investigation to their potential in inducing ground plane currents when included in an antenna design that is placed over a large ground plane. With the ability to excite ground plane currents on metallic structures, the investigated antenna can improve the performance of electrically small antennas through strategic placement. This antenna is what is used as the feeding mechanism for the proposed edge treatments so their behavior is accurately characterized.

Chapter 1

Introduction

1.1 Motivation

The standard whip antenna is a widely used electrically small antenna for lower frequency communication channels. The simplicity in its design and operation make the whip antenna a popular candidate if the form factor and agile mobility of the antenna platform is not of utmost concern. However, the whip antenna can quickly become cumbersome if designed for a mobile platform that circumstantially enters physically cluttered environments which inhibits the platform's mobility. A previously investigated electrically small placement insensitive antenna designed for RFID applications [1] is an ideal candidate to replace the whip antenna. The placement insensitive antenna can achieve the same performance as the whip antenna, but it possesses a planar, more compact, and non-protrusive profile that makes it better suited for mobile antenna solutions.

The placement insensitive antenna is an electrically small, dielectrically-backed, spiral inductor-loaded slot antenna with ground plane edges treated with triangular serrations. The benefit of this design is that it allows the antenna to be placed on any flat surface of arbitrary material properties without experiencing performance degradation. An example for one design of this antenna is shown at the top of Fig-

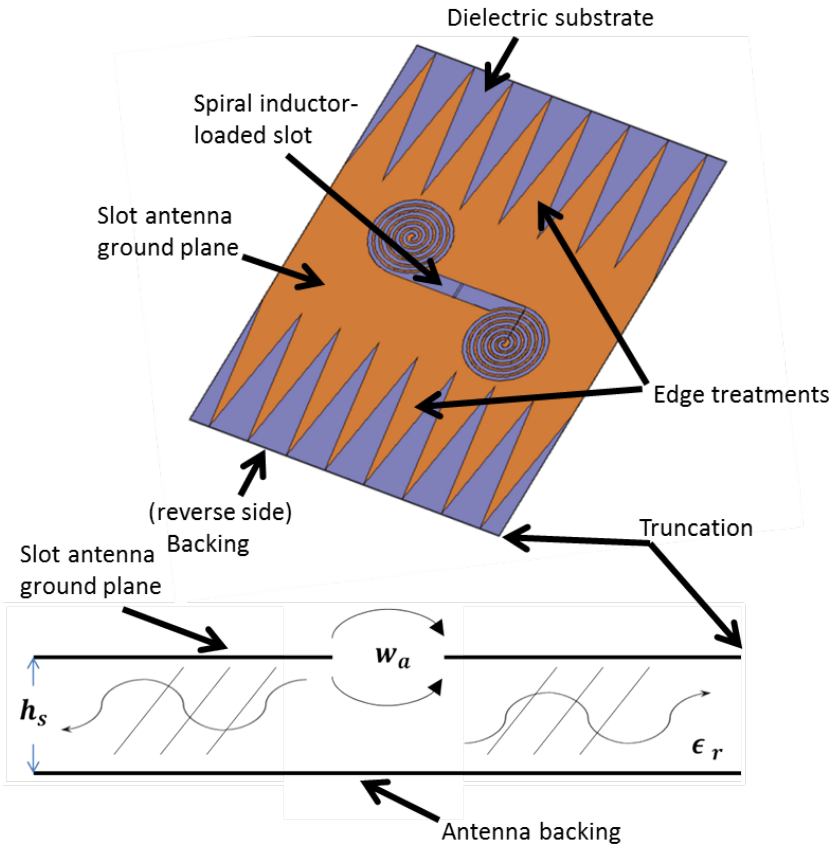


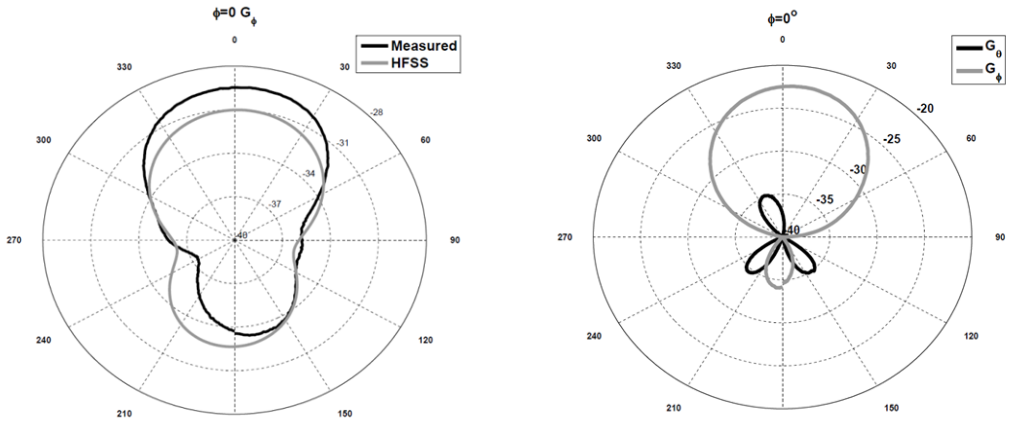
Figure 1.1: (Top) Placement insensitive antenna; (Bottom) Slot fields coupling into parallel plate waveguide.

ure 1.1. The antenna is excited via transmission line at the center of the slot. When the antenna is placed on a surface, the slot fields couple into parallel plate waveguide modes between the slot ground plane and the antenna backing, as depicted at the bottom of Figure 1.1. If the antenna ground plane does not contain serrated edges, the parallel plate waveguide modes get reflected at the abrupt truncation of the antenna ground plane because the sharp discontinuity presents an impedance mismatch between the parallel plate and freespace. The reflected energy then couples back into the slot, effectively presenting an additional reactive loading element to the input impedance of the slot, which de-tunes the antenna and disrupts its operation. The presence of the serration edge treatment mitigates the reactive loading effect by matching the impedance of the parallel plate to freespace, thus allowing the parallel plate waveguide modes to escape from within the structure which then becomes the primary radiation mechanism for the antenna.

Since the triangular serrations already posses acceptable performance measures for the antenna's operation, other types of edge treatments were not previously considered. Thus, only the triangular serration edge treatments have been investigated for the placement insensitive antenna. In general, no other ground plane edge treatment types have been investigated.

A quarter of the way into the program, the author received fellowship sponsorship from the United States Air Force which shifted the overall research objective to be more relevant and applicable to the mission of the sponsor. Instead of choosing a new path of research, it was determined that research findings on edge treatments and the antenna structure they are to be implemented in may be re-purposed for determining the placement insensitive antenna as a potential candidate for improved aircraft communication capabilities.

It has been shown that the realized gain of the placement insensitive antenna,



(a) (b)

Figure 1.2: (a) Phi polarization of realized gain of placement insensitive antenna in the $\phi = 0$ cut plane when not containing backing ground plane (b) Theta and phi polarizations of realized gain of placement insensitive antenna in the $\phi = 0$ cut plane when containing backing ground plane.[1]

when coupling into a backing ground plane, experiences an increase [1]. Figure 1.2 illustrates the effect on the realized gain of the placement insensitive antenna when a backing ground plane is and is not present. This concept can be extended to considering an aircraft as being the backing ground plane for the antenna. Depending on the size and shape of the aircraft, however, use of the placement insensitive antenna is not readily applicable for one unavoidable reason. Aircraft bodies can possess very complex geometries that consequently present very complex electromagnetic environments. This makes antenna design for aircraft a more difficult task because of all the different ways the antenna's radiation can interact with the aircraft body. These interactions may become prominent enough to entirely alter the radiation behavior of the antenna. This has sparked much research into understanding the complex electromagnetic environment of aircraft bodies and how antennas interact with them.

Most research on aircraft antennas has been approached more from a perspec-

tive of scattering and diffraction that only served to characterize the environment in which a specific type of antenna interacts with [2]–[6]. This involved invoking special theories that characterize the phenomena, such as the Geometric or Physical Theory of Diffraction (GTD/PTD), Geometric or Physical Optics (GO/PO), and even the Method of Moments (MoM). Utilizing these methods, antenna designers would either use known antenna designs or design new types of antennas around maintaining aerodynamic specifications of the aircraft and then study their interaction with the aircraft. Advances in computing technologies allow this approach to provide very accurate answers, but it imposes limitations to the underlying context for choosing a specific antenna design that would be most desirable. The process usually involves more of a ”guess and check” optimization procedure for the antennas which can become time consuming and thus not very efficient.

Another perspective on the characterization of aircraft electromagnetic environments involves looking at current flow on the aircraft body. On top of all the scattering and diffraction that may occur, the near fields of an antenna mounted on the body can induce currents on the body that alters the radiation behavior of the antenna. Furthermore, invoking the Theory of Characteristic Modes [7]–[9] can provide insight into the inherent current modes supported by the aircraft body which can explain the interaction of the induced currents on the behavior of the radiation for an antenna on the aircraft body. In general, one can have a more characterized environment for radiation of the aircraft body without an antenna, so the antenna design and placement process may be approached more strategically [10]. Essentially, instead of taking a known antenna design and optimizing it based on its behavior on the aircraft, this new approach can provide insight into the inherent electromagnetic properties of the aircraft so antenna design and placement of the antenna can be synthesized around these properties, which even has the potential

to avoid some of the scattering phenomena that can take place for certain antenna types and their more arbitrary placements that arise from the other design methods.

The concept of current induction and characteristic modes can be extended to antenna design and placement strategies for electrically small antennas. Electrically small antennas are inherently inefficient radiators, but if the antenna is placed in a location of a desirable current distribution containing a high modal weighting according to the aircraft's characteristic modes, the antenna can act as a probe that couples into the aircraft body, inducing currents so the the aircraft body itself becomes the radiator instead of the antenna [11]. This can potentially increase the overall efficiency of the antenna. Given that the placement insensitive antenna, that is to be studied as a viable aircraft antenna, is electrically small, the principle of this antenna acting as a probe that excites currents on the aircraft body is of potential interest. However, determining the exact antenna structure to be mounted on an aircraft is out of the scope for this thesis. Instead, the antenna is to be studied in a more general case, namely the study of the antenna's ability to couple into a ground plane of simple rectangular shape.

This thesis details an investigation of viable edge treatment alternatives to the triangular serration edge treatment, for inclusion into the design of the electrically small placement insensitive antenna, that will enhance the edge treatment radiation performance and allow miniaturization of the antenna structure to a smaller form factor. The research further details the placement insensitive antenna containing alternative edge treatments as a viable electrically small excitation probe for purpose of controlling induced currents on a ground plane which enhances the radiation of the antenna compared to other antenna types that operate over or on a ground plane.

1.2 Thesis Outline

The thesis begins with introducing what edge treatments are and why they're important, followed by the parametric investigation of different edge treatment types and their relative performance characteristics. This will lead into Chapter 3, which was a side study that occurred as a result of an accidental error in one of the edge treatment simulation designs. This edge treatment produced an interesting result that merited further investigation. Chapter 4 introduces the potential of edge treatments for coupling into a ground plane so the ground plane either aids in the radiation or becomes the radiator itself. Chapter 5 shows measurements obtained for the fabricated antennas and ground plane, but also includes a brief survey of characteristic mode theory which was used for antenna placement on ground plane. Chapter 6 then covers overall conclusions and potential future direction that the research can take.

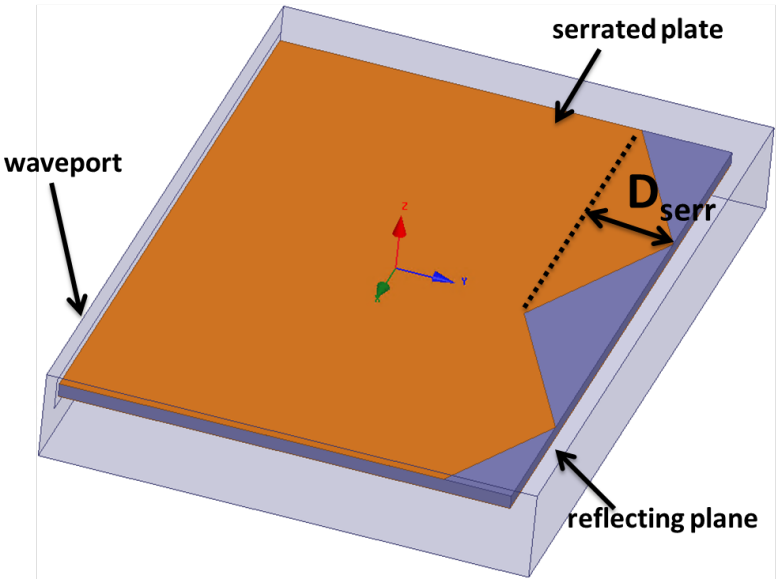
Chapter 2

Edge Treatment Variation Investigation

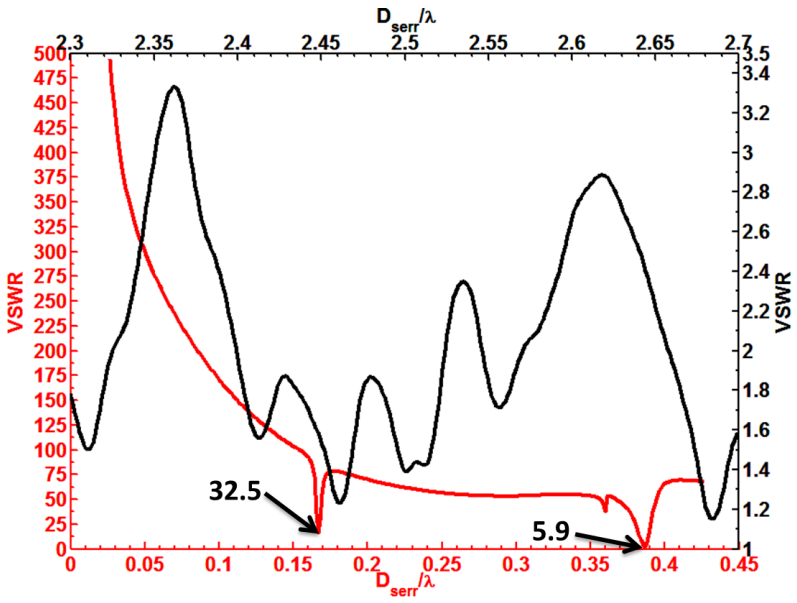
2.1 Introduction

Serrating an edge at the abrupt truncation of a parallel plate waveguide has been shown to minimize reflection at that plane and create a broad impedance match between the waveguide and freespace [1]. The greater the impedance match, the more power can be radiated from the parallel plate waveguide into space. This was shown to be important in the application it was previously used in. There are, however, fundamental limitations to this method, which adheres to the same limitations imposed on electrically small structures. More precisely, it is most effective when the parallel-plate and serration are an appreciable size of the wavelength at which the structure is operating at. Figure 2.1 illustrates this effect when the depth of the serration D_{serr} varies in electrical size. At large electrical sizes ($\sim 2.5\lambda$), the VSWR varies from about 1.2 to 3.4. When the serration depth approaches electrically smaller sizes ($\leq 0.5\lambda$), the VSWR increases drastically and approaches extremely large values when considered to be electrically small.

The overall goal of this investigation was to determine if such an edge treatment shape exists, other than a triangular serration, that is better at matching the impedance of an aperture coupled parallel plate waveguide to freespace when the



(a)



(b)

Figure 2.1: (a): Parallel plate waveguide with serrated edge, (b): VSWR of serrated parallel plate waveguide with various serration depth electrical sizes.

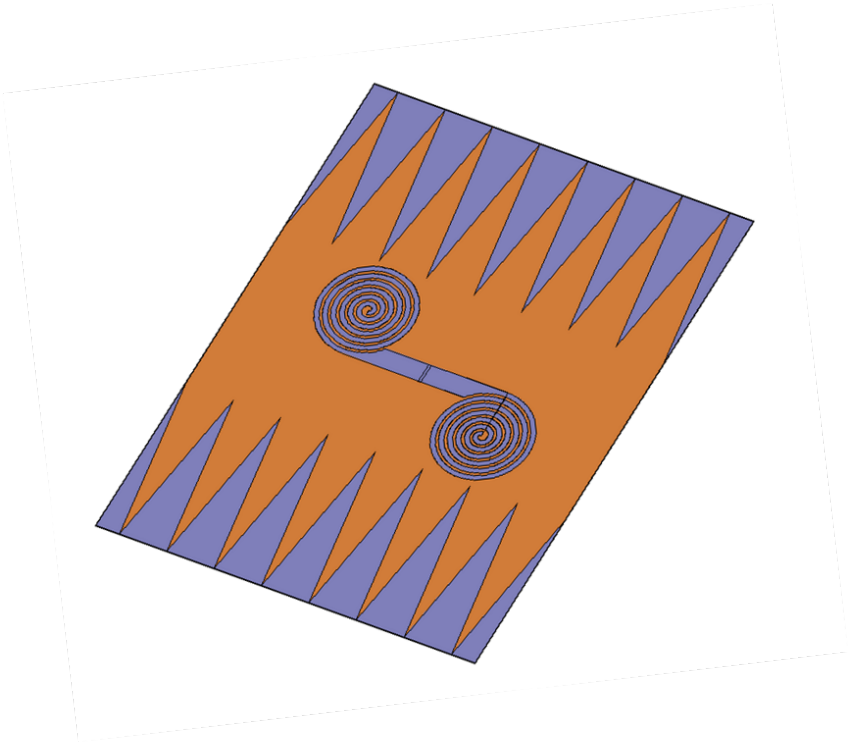
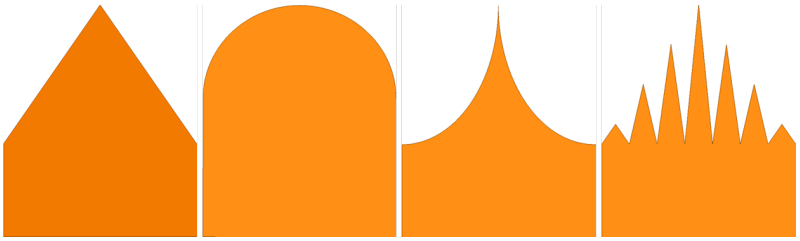
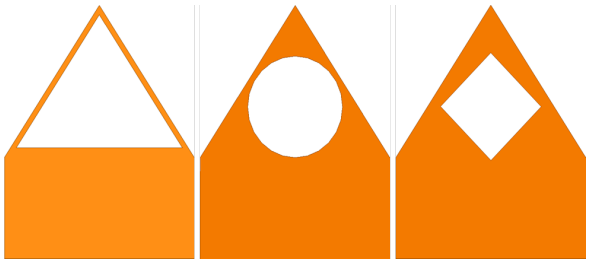


Figure 2.2: Placement insensitive antenna that different edge treatments are being studied for [1].

edge treatment is built into the edge of which the waveguide is to radiate from, particularly when the overall size of the structure is considered to be electrically small. Thus, the resulting impedance match would theoretically increase the efficiency of the structure as a radiator and ensure maximum power radiated from the structure. The edge treatment that possesses the most desirable performance characteristics would be considered for inclusion into the design of the placement insensitive antenna used for communication purposes mentioned in Chapter 1 and will be the antenna used to test and obtain measurements of the edge treatments later on.



(a)



(b)

Figure 2.3: (a)Left to right: triangular serration, half-circle serration, curved serration, subtriangular serration. (b)Left to right: triangular aperture, circular aperture, diamond aperture.

2.2 Comparison of Different Structures

The triangular serration edge treatment itself is favorable in its performance, thus other candidates for edge treatment shapes similar to the triangle were considered. These other shapes are pictured side-by-side in Figure 2.3(a). Among these other shapes there is the half-circle serration which is a series of adjacent half-circles of equal radius, the curved serration which is a series of adjacent triangular shapes but with two of its edges curving exponentially and converging to a vertex, and the subtriangular serration which is a series of adjacent thinner triangles with equal widths and with heights staggered so their vertices trace out two edges of a triangle of greater width. The half-circle and curved serrations were considered due to their curved geometries which are generally favorable for structures operating at radio frequencies. The subtriangle serrations were considered due to their potential

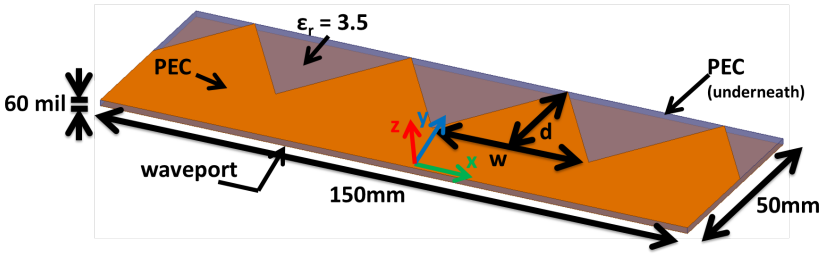


Figure 2.4: Parallel plate structure under consideration. Serrated edges are base model used for comparison.

broadband matching characteristics.

In addition to different edge treatment shapes, leakage-enhancing apertures cut out of the edge treatment were considered due to the intuition that the apertures would become an additional source of radiation, contributing to the overall amount of power to be radiated from the edge treatments. Aperture shapes considered are shown in Figure 2.3(b). The apertures are cut out of the triangular serration edge treatment to evaluate their effectiveness at increasing the total power radiated when compared to the unaltered triangular serration. Aperture shapes considered were a triangle with side lengths proportional to the side lengths of the triangular serration, a circle, and an equilateral diamond. All apertures are centered about the triangular serration.

A base structure used for the comparison consisting of the unaltered triangular serration edge treatment was constructed in HFSS. This structure is shown in Figure 2.4. The rectangular parallel plate dimensions and relative dielectric constant of the substrate between the plates are kept constant while the dimensions of each edge treatment or aperture are varied. The width and length of the structure are 150 mm and 50 mm respectively while the height of the substrate is 60 mil. The width w and depth d of an edge treatment are the dependent variables in this study. The top and bottom plates are modeled with a perfect electric conductor boundary

condition and the substrate is Dupont Type 100 HN Film with relative permittivity of 3.5. The structure is excited with y-directed TEM wave from a waveport in the XZ-plane, on the side opposite to the edge treatments, as indicated in Figure 2.4. A large parametric investigation through HFSS simulations was initiated which compared the impedance matching and radiating capabilities of each of the proposed edge treatment variations. Analysis includes observing the VSWR, peak realized gain, power radiated, and realized gain for both theta and phi polarizations in the principle cut planes. Observations are made with special interest when the structure is electrically small.

2.3 Performance Analysis

Initial analysis focused on keeping width and depth of each edge treatment constant, where $w = 40mm$ and $d = 30mm$, and comparing the performance of each edge treatment at these dimensions. Additionally, each aperture is included in the comparison and chosen to be an almost maximum dimension so the aperture does not become fully inscribed on the edge treatment.

The VSWR of each structure is presented in Figure 2.5. The minima for each curve appears near series resonances and represents a relative impedance match. Although most minima still occupy large values, the definition of these impedance matches are relative to the edge treatment's inherent capabilities as an impedance matching structure. Additionally, as the structure enters electrically small dimensions, large impedance mismatches are due to very high reactive impedances that are intrinsic characteristics of electrically small structures.

The base model with triangular serrations (blue curve) shows to possess an impedance match when the structure is very near to being considered electrically

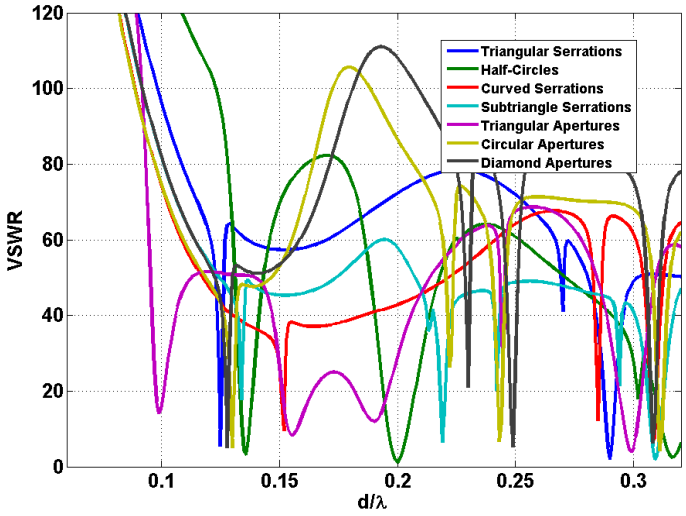


Figure 2.5: VSWR of each structure at $w = 40mm$ and $d = 30mm$. The abscissa is the depth of the edge treatment normalized to free space wavelength. Apertures are at dimensions $0.875d$, $0.667d$, and $0.5303d$ respectively in the order as shown in legend

small followed by another impedance match when the structure is close to a quarter wavelength in length. The other structures follow a rather similar trend but to varying degrees. The structure with the half-circle edge treatment (green curve) exhibits more broadband characteristics as evident from wider impedance match minima, but fails to match at a smaller electrical length. The curved serration edge treatment (red curve) does not provide any real benefit in regards to its impedance matching capability but provides slightly more favorable radiation characteristics which will be discussed later. The subtriangle serration edge treatment (cyan curve), over the entire band observed, possesses the lowest average VSWR due to the multiple impedance matches it experiences. The subtriangles have multiple matches due to its more complex geometry presenting more accommodating electrical sizes for the structure to resonate at, but still does not provide an impedance match at a smaller electrical size than the triangular serration.

Edge Treatment	d_{serr}/λ_0	$VSWR_{min}$
Triangular	0.13	5.34
Half-cricle	0.14	3.10
Curved	0.15	9.53
Subtriangular	0.13	17.8
Triangular Ap.	0.10	14.1
Circular Ap.	0.13	4.99
Diamond Ap.	0.13	5.08

Table 2.1: VSWR minima observed for each edge treatment for the electrically small case.

The edge treatments containing the circular and diamond apertures (gold curve and dark grey curve respectably) appear to be better suited once the dimensions start to approach a quarter wavelength. The effect of impedance matching is negligible at the smaller electrical sizes for these structures including a large mismatch occurring right before entering a quarter wavelength in length. The most intriguing result observed from Figure 2.5 belongs to the structure with triangular apertures[1] (purple curve). An impedance match occurs when the structure is electrically small ($d = \frac{\lambda}{10}$) and further possesses fairly broadband characteristics at the smaller electrical sizes. The behavior of the impedance match starts to follow a more regular pattern similar to the other apertures as the electrical size of the apertures approaches a quarter of a wavelength.

Disregarding the data for the triangular aperture edge treatment, for the reason mentioned in the footnote, none of the edge treatments show appreciable impedance matching improvement over the base case at electrically small sizes. Particularly, adding an aperture does not show possess the possibility for miniaturization. The

[1]The data obtained for this structure was obtained in error. The HFSS structure for this case contains disconnected aperture arms at for the serrations at both endfire locations of the structure. Due to the nature of this result, after the cause for this error was determined, this result merited further investigation and thus is elaborated on later in Chapter 3.

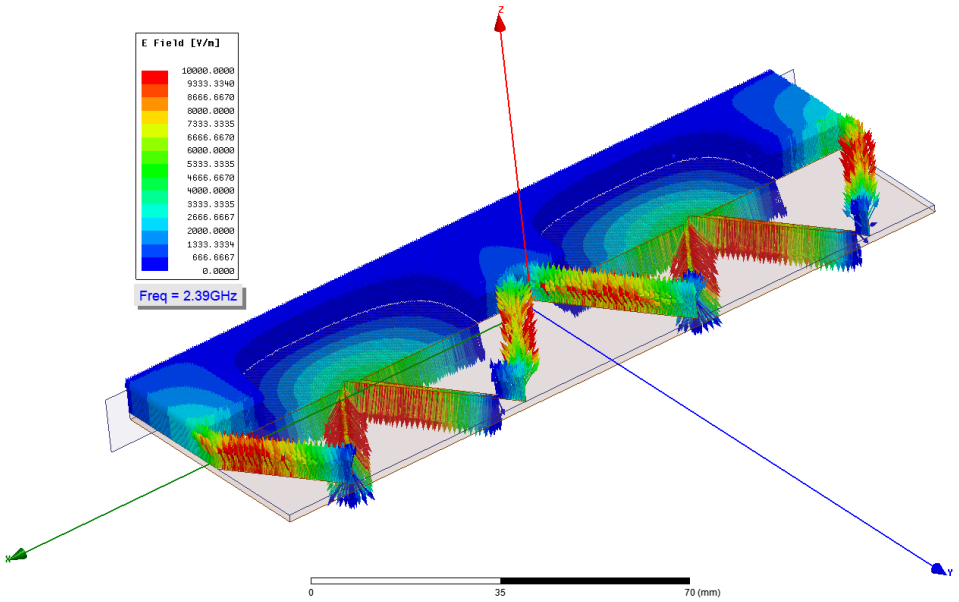


Figure 2.6: Vector electric fields plotted on the HFSS model for the structure containing triangular aperture edge treatments which show the existence of a higher order mode on the structure.

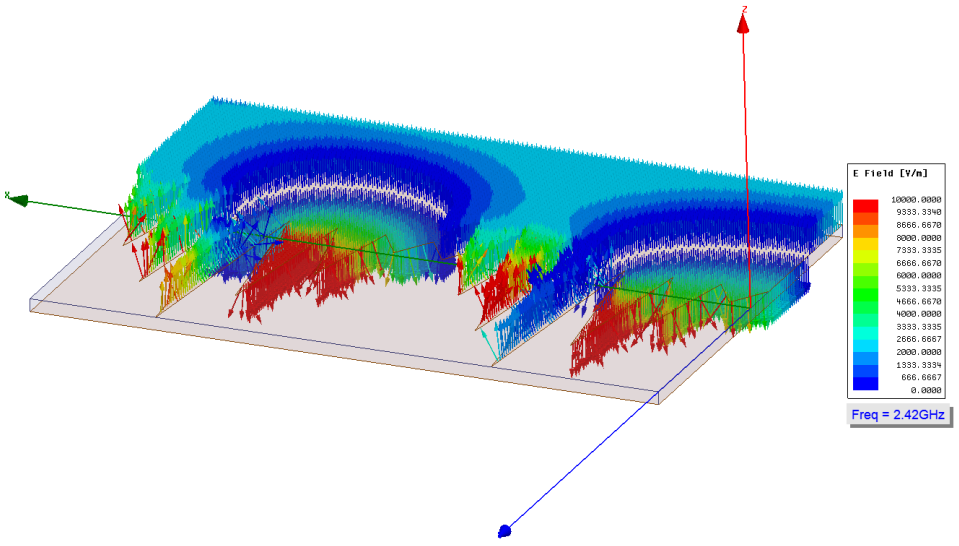


Figure 2.7: Vector electric fields plotted on the HFSS model for the structure containing subtriangular edge treatments which show the existence of a higher order mode on the structure.

salient characteristics for the edge treatments at the electrically small case are listed in Table 2.1. In terms of bandwidth, the half-circle edge treatment offers the most, due to its overall larger electrical size compared to the other edge treatments. Once the edge treatment serration depths start approaching electrical sizes larger than a fifth of a wavelength, the impedance matching behavior starts to become more sporadic. At larger electrical sizes, higher order modes start to exist within the structure. The junction between the parallel plate and edge treatment does not create a perfectly smooth transition so the source TEM wave experiences diffraction and scattering phenomena occurring at the discontinuities. The type of diffraction and scattering is highly dependent on the edge treatments' electrical size and geometry. The higher order modes can consequently introduce different environments for which the edge treatment fringing fields couple into with each other. Examples of a higher order modes existing on the subtriangular edge treatment and triangular aperture edge treatment (not containing disconnected aperture arms) are shown in Figures 2.7 and 2.6 respectively. This deviation from true TEM radiation accounts for the sporadic multi-band behavior of each of the edge treatments.

The peak realized gain in dB for each structure is presented in Figure 2.8. As is immediately evident, minima in VSWR from Figure 2.5 correspond to maxima in the peak realized gain in Figure 2.8. The half-circle edge treatment shows to possess the largest peak realized gain out of all the structures occurring over the sweep at points 0.2λ and about 0.32λ. The curved serrations edge treatment, over the entire band observed, possesses the greatest average peak realized gain and remains fairly constant starting after around 0.15λ, but is distinctly lacking in larger peak values. The subtriangle serrations show a rather sporadic peak realized gain that becomes difficult to characterize due to its more complex geometry, but tight coupling between adjacent serrations during the structures many resonances could

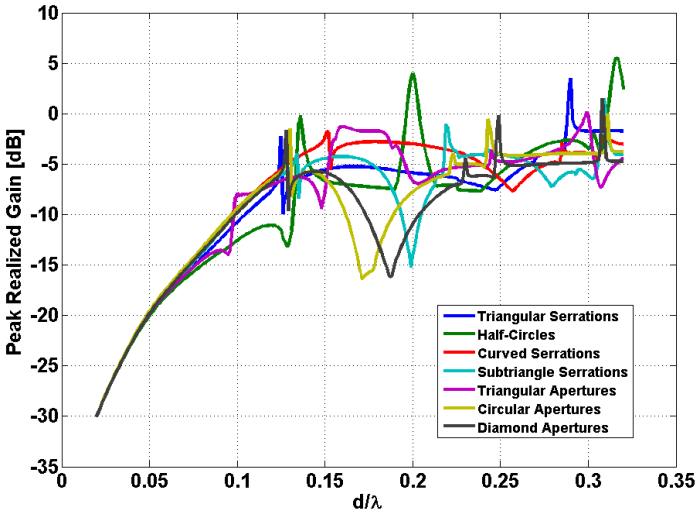


Figure 2.8: Peak realized gain in dB of each structure from Figure 2.5.

account for the rather smaller overall peak realized gain. The peak realized gain of both the circular and diamond aperture edge treatment structures is reflected by their impedance matching performance with maxima and minima of the gain lining up with corresponding minima and maxima respectively of their VSWR. The triangular aperture edge treatment has an increase in peak realized gain at 0.1λ, which is greater than the other structures, from its impedance match at the same electrical size.

The power radiated in dBm for each structure is presented in Figure 2.9. The trends in power radiated for each structure follow very closely with the trends in their peak realized gain, but scaled to the different units. The half-circle edge treatment, at one instance occurring when the structure is about a fifth of a wavelength in electrical size, radiates the most power of any structure at any instance across the whole band analyzed; but the peak goes above 30 dBm which appears to be an error in simulation convergence because the amount of input power to the structure is nominally 1 Watt. The triangular aperture edge treatment radiates the most power

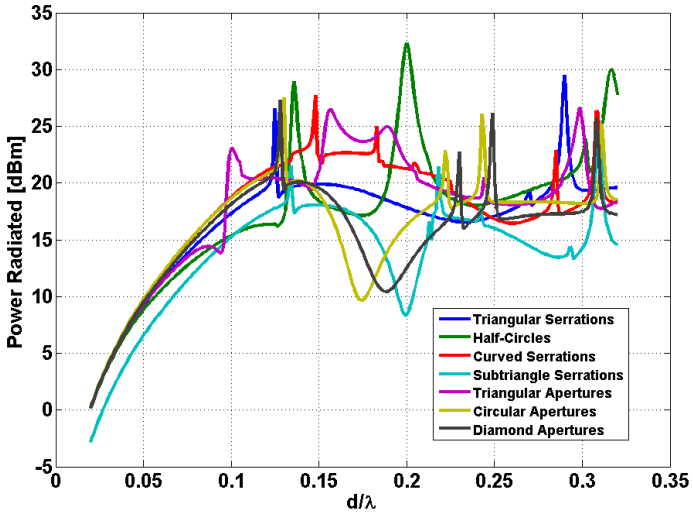


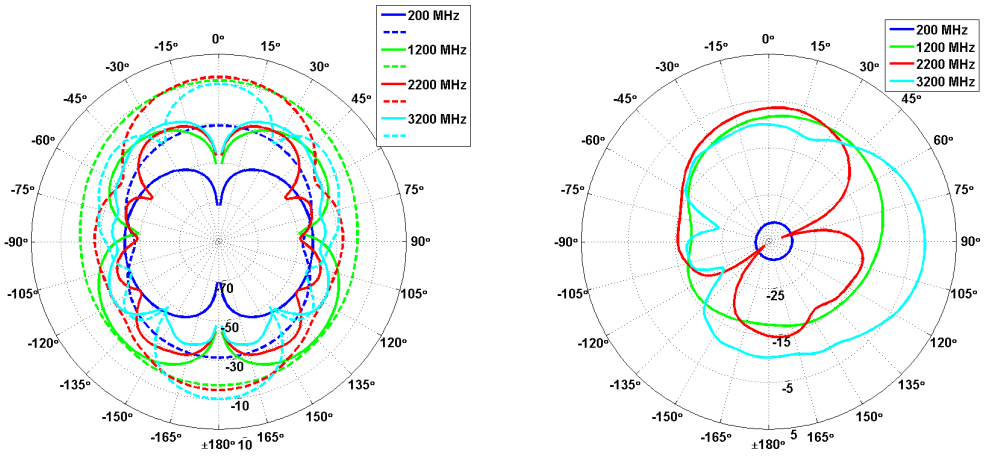
Figure 2.9: Total power radiated in dBm of each structure from Figure 2.5.

when electrically small.

2.4 Radiation Patterns

Figures 2.10 - 2.23 show the two dimensional radiation patterns of realized gain for each structure at the same edge treatment dimensions as those used in the VSWR, gain and power radiated analysis. The patterns include both Θ and Φ polarizations for the $\Phi = 0°$, $\Phi = 90°$, and $\Theta = 90°$ cut planes at following frequency points: 200 MHz, 1200 MHz, 2200 MHz, and 3200 MHz which correspond to electrical lengths of 0.02λ, 0.12λ, 0.22λ, 0.32λ respectively. For the $\Phi = 90°$-cut plane of every structure, the Φ-polarization is negligible and thus not included so as to emphasize deviations in the Θ-polarization among the different structures and their electrical lengths.

Subfigure (b) of Figures 2.10,2.12,2.14,2.16,2.18,2.20,2.22 show the Θ-polarization realized gain of each structure in the $\Phi = 90°$ cut plane. For each structure, the smallest electrical length (blue pattern) has a very small realized gain, producing a



(a) (b)

Figure 2.10: Realized Gain of triangular serrations across Θ for both polarizations. Θ-polarization is represented by the solid lines and Φ-polarization is represented by the dashed lines.

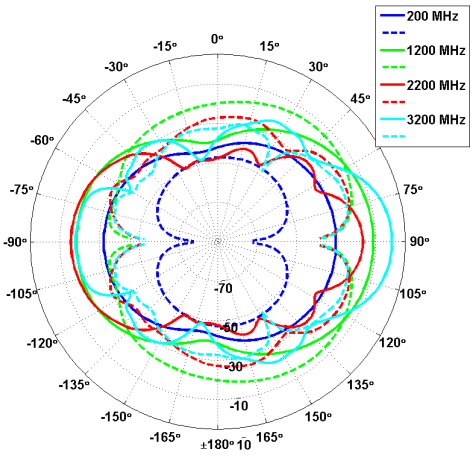
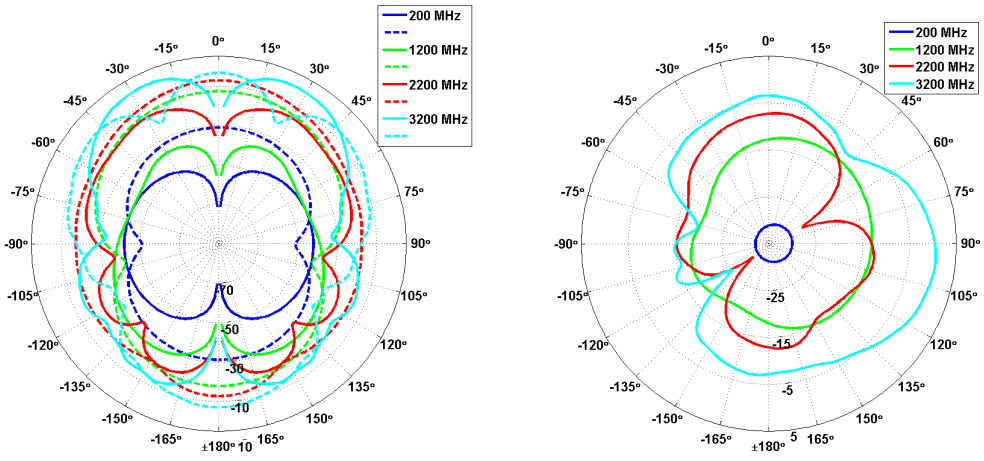


Figure 2.11: Realized Gain of triangular serrations across Φ for both polarizatoins. Θ-polarization is represented by the solid lines and Φ-polarization is represented by the dashed lines.



(a) (b)

Figure 2.12: Realized Gain of half-circles across Θ for both polarizations. Θ-polarization is represented by the solid lines and Φ-polarization is represented by the dashed lines.

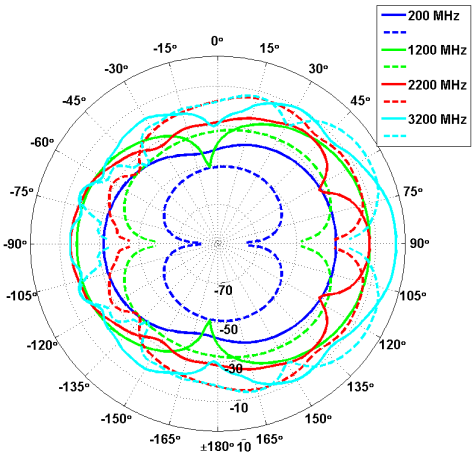
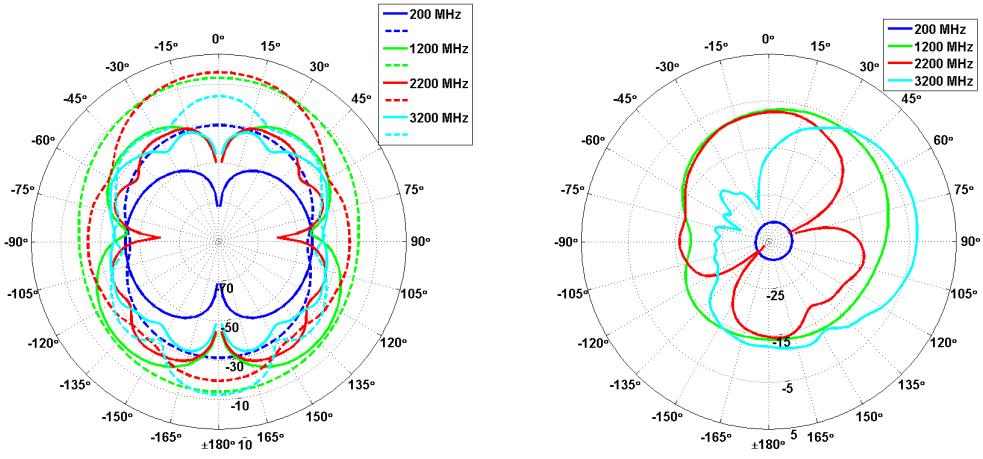


Figure 2.13: Realized Gain of half-circles across Φ for both polarizatoins. Θ-polarization is represented by the solid lines and Φ-polarization is represented by the dashed lines.



(a) (b)

Figure 2.14: Realized Gain of curved serrations across Θ for both polarizations. Θ-polarization is represented by the solid lines and Φ-polarization is represented by the dashed lines.

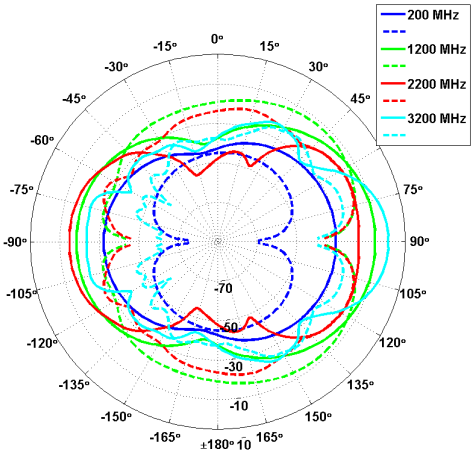
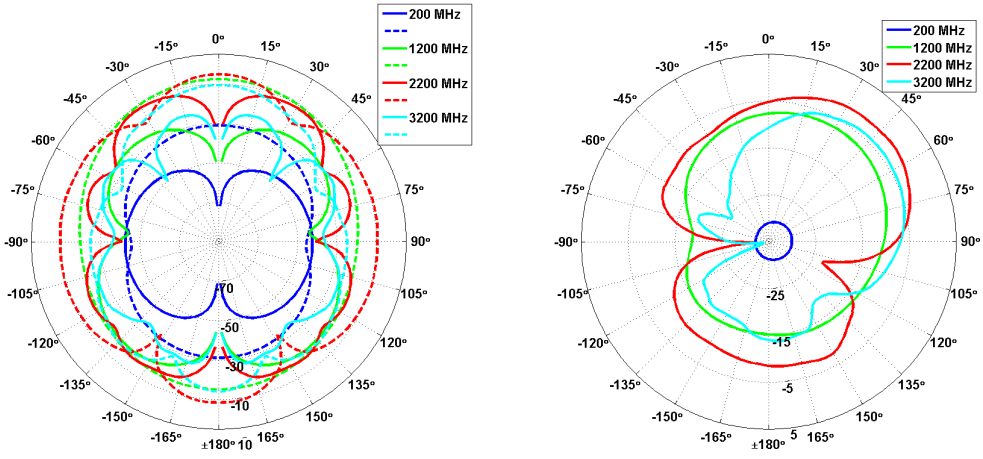


Figure 2.15: Realized Gain of curved serrations across Φ for both polarizatoins. Θ-polarization is represented by the solid lines and Φ-polarization is represented by the dashed lines.



(a) (b)

Figure 2.16: Realized Gain of subtriangular serrations across Θ for both polarizations. Θ-polarization is represented by the solid lines and Φ-polarization is represented by the dashed lines.

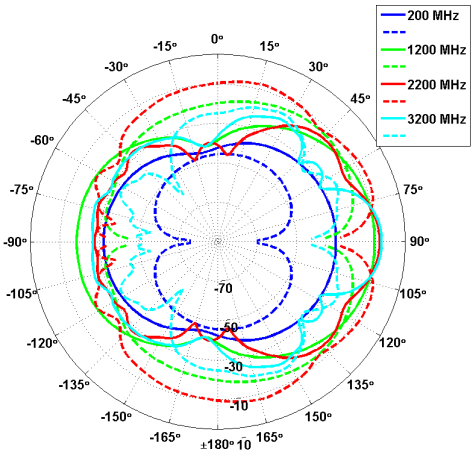
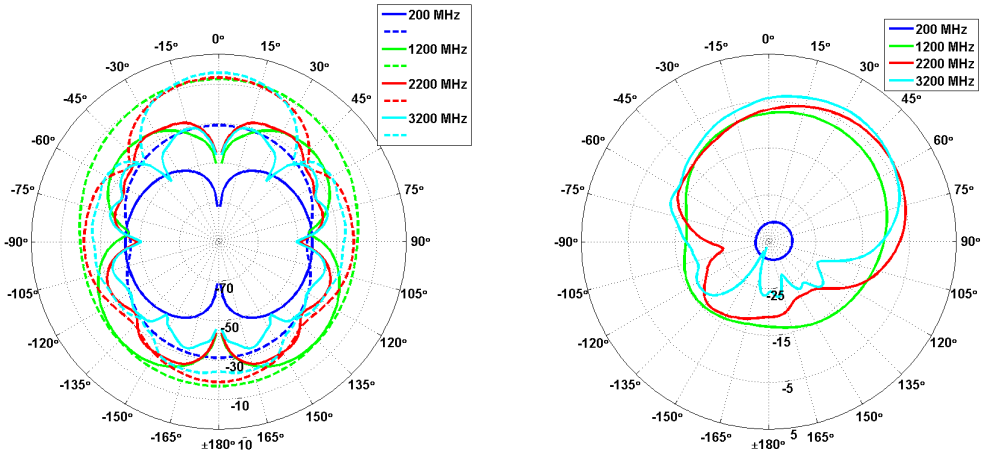


Figure 2.17: Realized Gain of subtriangular serrations across Φ for both polarizatoins. Θ-polarization is represented by the solid lines and Φ-polarization is represented by the dashed lines.



(a) (b)

Figure 2.18: Realized Gain of triangular serrations with triangular apertures across Θ for both polarizations. Θ-polarization is represented by the solid lines and Φ-polarization is represented by the dashed lines.

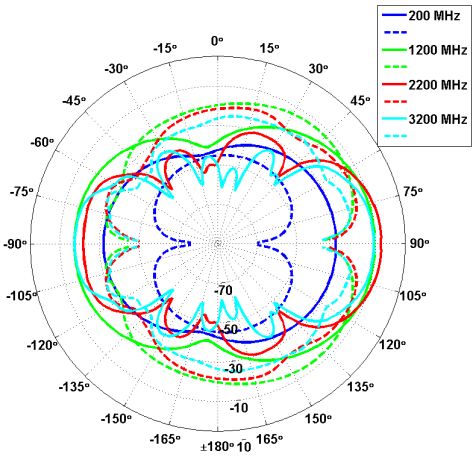
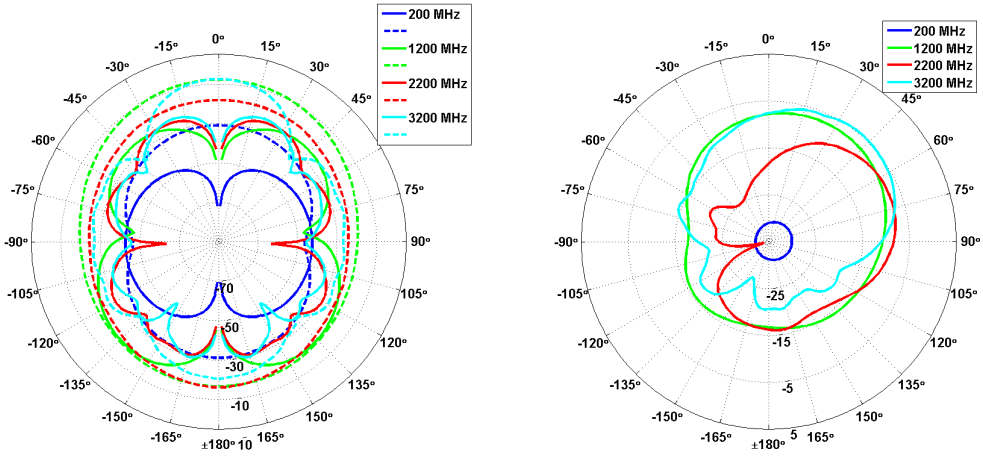


Figure 2.19: Realized Gain of triangular serrations with triangular apertures across Φ for both polarizatoins. Θ-polarization is represented by the solid lines and Φ-polarization is represented by the dashed lines.



(a) (b)

Figure 2.20: Realized Gain of triangular serrations with diamond apertures across Θ for both polarizations. Θ-polarization is represented by the solid lines and Φ-polarization is represented by the dashed lines.

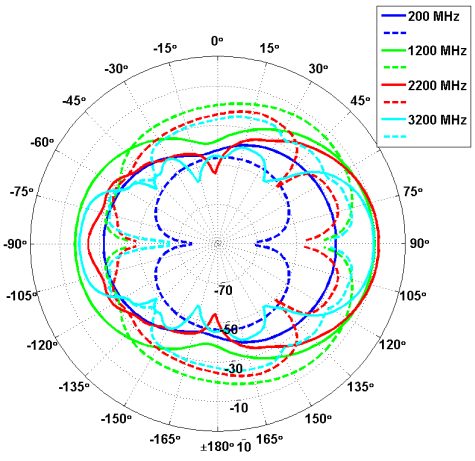
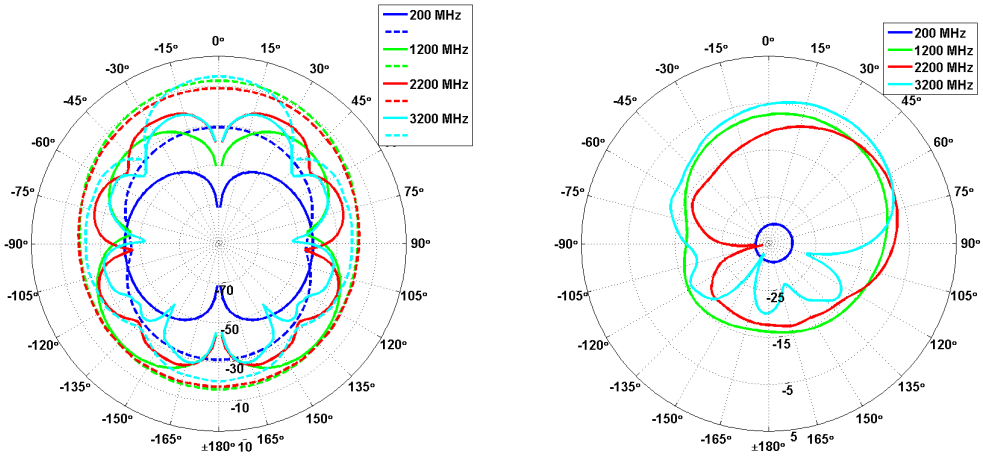


Figure 2.21: Realized Gain of triangular serrations with diamond apertures across Φ for both polarizatoins. Θ-polarization is represented by the solid lines and Φ-polarization is represented by the dashed lines.



(a) (b)

Figure 2.22: Realized Gain of triangular serrations with circle apertures across Θ for both polarizations. Θ-polarization is represented by the solid lines and Φ-polarization is represented by the dashed lines.

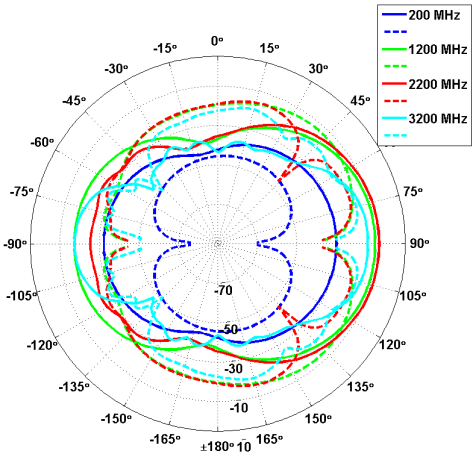


Figure 2.23: Realized Gain of triangular serrations with circle apertures across Φ for both polarizatoins. Θ-polarization is represented by the solid lines and Φ-polarization is represented by the dashed lines.

radiation pattern similar to that of a Hertzian dipole rotated 90°, which is consistent with the radiation characteristics of an electrically small antenna. As each structure starts to approach a size that is more appreciable of a wavelength, the realized gain increases.

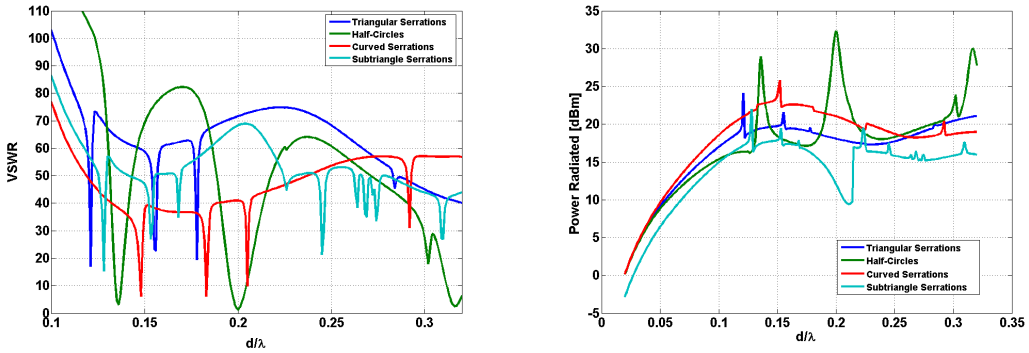
The structures without an aperture all possess similar radiation patterns with the largest electrical size (cyan pattern) producing the highest realized gain broadside to the structure. When each structure is about a quarter of a wavelength (red pattern), nulls start to appear close to broadside and endfire radiation becomes more pronounced. The structures' radiation patterns containing apertures in the edge treatment show more constant or uniform realized gain across frequency, when compared to the base structure without the apertures. With the electrically small structure the realized gain is still very small, but when each structure starts to approach a size that is more appreciable of a wavelength the broadside gain for each subsequent electrical size is approximately the same. This shows that the apertures do influence the overall radiation characteristics of an edge treatment, which is particularly evident by what happens when the edge treatment is approximately a quarter-wavelength. The broadside nulls are mitigated showing that the apertures promote fields to radiate more uniformly as opposed to just from edge treatment or waveguide truncation itself.

The general behavior of each edge treatments' radiation patterns can be summarized as follows: Broadside radiation is primarily theta-polarized; end-fire radiation is more phi-polarized - this is true in general and does not depend on setup. The way an edge treatment radiates at a certain frequency is dependent on these conditions: electrical size of the edge treatment, geometry of the edge treatment, and VSWR of the edge treatment. At large electrical sizes ($d_{serr} = 2\lambda$), the VSWR is significantly low, but higher order modes prevail and the edge treatment gets very

directive, multi-lobe radiation patterns. Behavior at smaller electrical sizes is dictated more by geometry. Smooth geometries result in less diffraction which results in smoother radiation characteristics. Jagged geometries result in more diffraction/scattering inside and outside the parallel plate structure. This results in the higher order modes existing within the parallel plate structure. These higher order modes create a different environment for which the edge treatments can then couple with each other, which is particularly evident for the subtriangular serration edge treatment. The VSWR at a particular frequency can also have an effect. Higher VSWR results in more field addition/cancellation inside the structure, which then provides higher order cavity modes that dominate in the radiation mechanism. In general, radiation is not constant/uniform across frequency unless TEM is the dominant mode in the structure. Proper selection of aperture can possibly promote more constant radiation. In general, if the radiation pattern is more important, consideration of edge treatments with more smooth, curved features - particularly the half circle or ellipse shaped edge treatments - should be included in the design. If possessing multi-band behavior is more important, consideration of use of edge treatments with more jagged, triangular shapes in the design would be more useful.

2.5 VSWR and Power Radiated - Additional Cases

The VSWR and power radiated for only unaltered edge treatments, this time with dimensions $w = 20mm$ and $d = 30mm$, are presented in Figures 2.24(a) and 2.24(b) respectively. The triangular serrations edge treatment's most distinguishable performance change from the base model is that two additional relative impedance matches occur before the structure becomes a fifth of a wavelength in length. The power radiated corresponding to these two additional impedance matches are rather

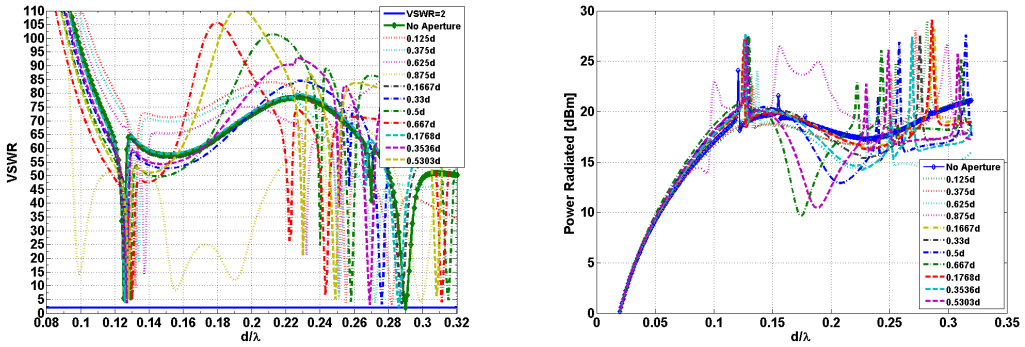


(a) (b)

Figure 2.24: VSWR and Power radiated in dBm for for different edge treatment dimensions with no apertures. Edge treatment width and depth are $w = 20mm$ and $d = 30mm$.

negligible due to the still high values of these VSWR minima. There is virtually no change in the performance of the half-circles edge treatment at this smaller dimension due to their still large overall electrical size, but the curved and subtriangle serrations exhibit a noticeable performance change. The first minima in the VSWR of the curved serration shifts down in electrical size and two additional impedance matches occur before the structure reaches a quarter wavelength in length. The subtriangle serrations edge treatment appears to show many VSWR minima. This is likely due to the amount of extra triangles that get implemented on the edge treatment as a result of the edge treatment width decrease which then creates a more complex coupling network between each triangle. All these additional minima, however, still occupy large VSWRs and thus contribute very little to the increase of overall power radiated at those corresponding electrical sizes.

The VSWR and power radiated for additional aperture sizes on the triangular serration edge treatment with base model dimensions are presented in Figures 2.25(a) and 2.25(b) respectively. A reference line for a VSWR corresponding to 2 is plotted along with the VSWR of the edge treatment without an aperture to high-



(a) (b)

Figure 2.25: VSWR and Power radiated in dBm for only structures with apertures. Edge treatment width and depth are $w = 40mm$ and $d = 30mm$. Dashed lines represent triangular apertures, dash-dot lines represent circle apertures, and dashed lines represent diamond apertures.

light the effect of adding the apertures. For the reference unaltered edge treatment, the first minima in VSWR occurs when the electrical size is about 0.13λ which is not quite electrically small yet. Adding apertures shows to have almost no effect on shifting the impedance match to a smaller electrical size with the exception of the triangular aperture at $0.875d$ experiencing an impedance match when the structure is electrically small as shown from the previous analysis. Otherwise impedance matches are unaffected until the structure becomes closer to a quarter wavelength in length. At the larger electrical sizes, the overall geometry and electrical size of the aperture will determine the degree of which the edge treatment experiences a shift in impedance match relative to the case of no apertures.

2.6 Conclusions

A parametric investigation on seven different edge treatment types was completed. Three of the candidates included a half-circle serration, a curved serration, and a subtriangular serration. Three additional candidates included apertures cut out of

the triangular serration in the shapes of a triangle, a circle, and a diamond. Analysis of each edge treatments impedance matching capability has shown that there is negligible improvement in VSWR when the type of edge treatment is changed. If broader bandwidth is desired, however, it would be of interest to select the half-circle edge treatment due to its smoother and larger overall electrical size. At larger electrical sizes, higher order modes occur which introduce multi-band behavior for the edge treatments containing more complex geometries, but the bandwidth for each of the impedance matches are narrow. The existence of higher order modes also reflect on the overall radiation mechanism of each edge treatment. For more complex coupling environments, edge treatments such as the subtriangular serration may experience stronger coupling which results in more stored fields than radiated fields. Conversely, the inclusion of apertures in the edge treatment promote more constant and uniform radiation characteristics across electrical sizes. No measured data was obtained for each edge treatment because obtaining measurements consistent with the simulation setup is no trivial task. Obtaining measurements requires a feed structure for the edge treatments, which in the case for this thesis, is obtained by inclusion of the edge treatments in the placement insensitive antenna.

Chapter 3

Side Study on Disconnected Apertures

3.1 Introduction

Referring back to data obtained from the simulations in Chapter 2, the triangular serration edge treatment structure with triangular apertures produced an interesting result. The VSWR corresponding to the largest aperture size dipped to a significantly lower value than all of its counterparts when the edge treatment was considered electrically small.

The cause of this phenomena was due to an accidental error in the HFSS modeling. Inspection into the HFSS model led to the discovery that the triangular aperture HFSS structure had aperture edges that were disconnected on the outside serrations of the structure. Nominally, the aperture was designed to parametrically contain continuity for an outside serration that gets cut off based on its width; but what resulted is, in effect, an L-bend arm resembling a microstrip line that stems abruptly from parallel-plate waveguide. An example of this structure, when the serration length and width are 49mm and 40mm respectively, is shown in Figure 3.1, with a magnetic wall boundary condition placed in the YZ-plane to mirror the structure across that plane.

Given the nature of this accidental result, it seemed pertinent to the goal of the

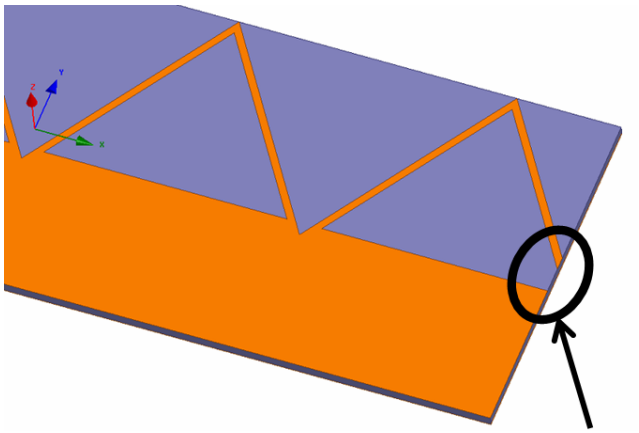


Figure 3.1: HFSS model of the triangular apertures edge treatment structure with disconnected aperture.

edge treatment study to investigate this phenomenon further. This chapter includes parametric simulations in HFSS were completed to show trends that provide insight into the behavior, followed by a transmission line model that was derived for the structure so accurate characterization of the structure can be made possible.

3.2 Changing Disconnected Arm Length

Since the initial observation was that the accidental structure produced a greater impedance match and power radiated at lower frequencies, a parametric investigation was completed to examine the effects of changing the length of the disconnected aperture arm. First, The depth of the serration and aperture were varied while keeping their widths constant. This allowed an effective increase in the length of the arm. Serration depths chosen where 10, 20, 30, 40, and 49 mm with a serration width of 40 mm. These dimensions produce an arm length of approximately 37.8, 47.8, 60.9, 75.4, and 89.3 mm respectively. To increase the arm length even further, the serration width was increased to 90 mm with a serration depth of 49 mm. This produces an arm length of about 107.2 mm, but also due to the parametrization of

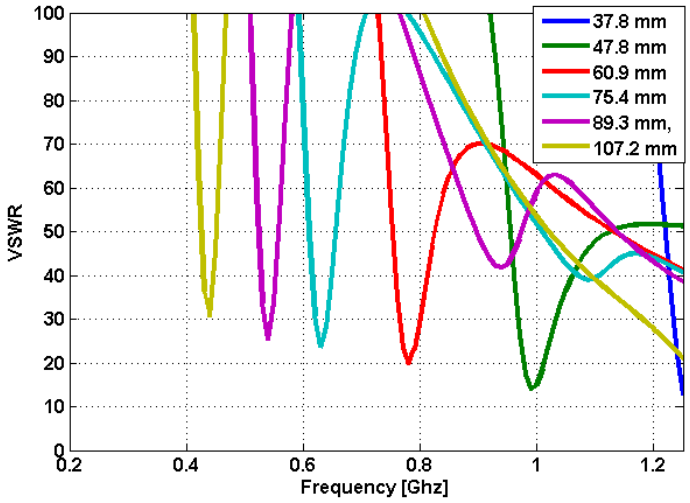


Figure 3.2: VSWR of each structure across frequency. Each curve represents a different arm length. As arm length ncreases, dip in VSWR shifts down in frequency.

the HFSS model the structure contains only the arm bends and no aperture edge treatments in between.

The VSWR of each structure with varying arm length when swept across frequency is shown in Figure 3.2. The primary objective is to provide a good impedance match from the waveguide to freespace which would correspond to a very low VSWR at frequencies of interest. The overall size of the structure enters an electrically small dimension when entering the operation at the middle hundreds of MHz and becomes detrimental to the efficiency of the structure as a radiator. As Figure 3.2 shows, increasing the length of the L-bend arm creates a much more appreciable impedance match as the overall structure becomes electrically smaller although the VSWR is still too high for practical use due to the small electrical size. Given the smaller overall electrical sizes at the lower frequency matches, there also is not much happening in the way of the disconnected arm structure creating a broadband impedance match; that is, until the overall electrical size increases. The bandwidth of the match steadily increases as the overall electrical size increases.

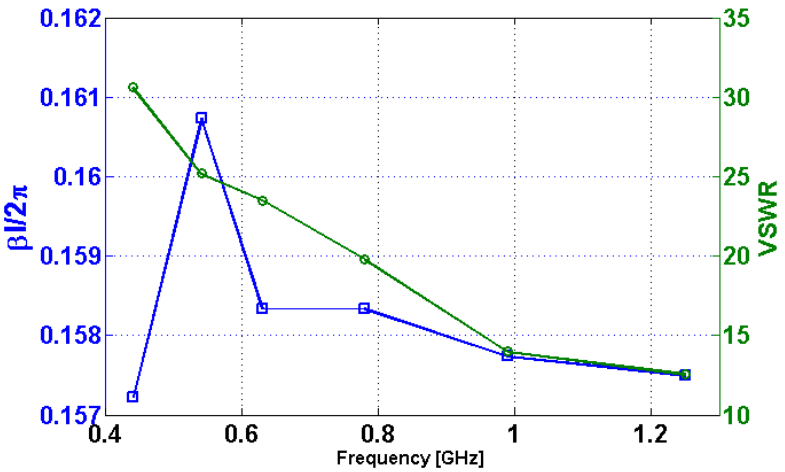


Figure 3.3: The frequencies at which the arm lengths experience impedance matches and their corresponding normalized electrical length.

There is a parallel resonance at each of the dips in VSWR which possess a relatively high resistance which can be attributed to the aforementioned impedance mismatch. Before each structure experiences its first resonance, the VSWR increases rapidly as the frequency decreases.

The VSWR value for each dip in the VSWR curves along with their corresponding frequency points and electrical lengths is plotted in Figure 3.3. The figure shows that even though increasing the length of the arm produces a relative impedance match, the VSWR increases slightly with each incremental increase in arm length. The accuracy of producing the correct electrical length for each impedance match increases in difficulty as wavelength increases, but the respective normalized electrical lengths show that the relative impedance matches all occur when the arm is about 0.1583λ, using free-space wavelength. Factoring the relative wavelength of the structure shows the electrical size of each of the arms to be about a third of a wavelength.

An important consequence from matching the impedance of the parallel plate

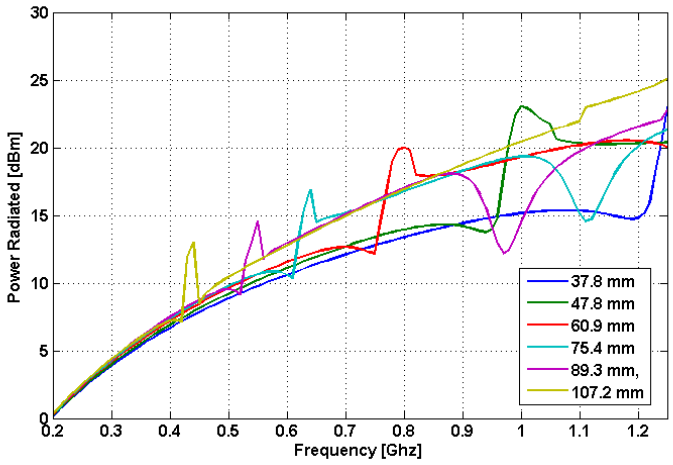


Figure 3.4: Total power radiated of each structure across frequency. Each curve represents a different arm length. A spike corresponding to an increased power radiated is shown to correspond with each structures' respective dip in VSWR.

guide to free space is to maximize the amount of power radiated from the structure. With a very low VSWR, full power radiated is possible - depending on the electrical size of the structure. This is shown in Figure 3.4. Initially, the power radiated is almost zero which corresponds to very low radiation efficiency of the structure when electrically small, but the power radiated otherwise gradually increases with increasing electrical size. The largest arm length has the greatest power radiated when averaged over the entire frequency sweep when compared to the shorter arm lengths. This is likely due to the largest arm length allowing for more accommodation of current flow when oscillating at higher frequencies. As the overall electrical size of the entire structure increases, however, the peak power radiated covers a wider swath of bandwidth as opposed to the smaller electrical sizes.

An important note for the phenomenon taking place is that the radiation mechanism for the structure is altered considerably from if the aperture arm wasn't disconnected. Actual apertures all across the edge treatments produce a more omnidirectional radiation pattern both in azimuth and elevation when the structure is

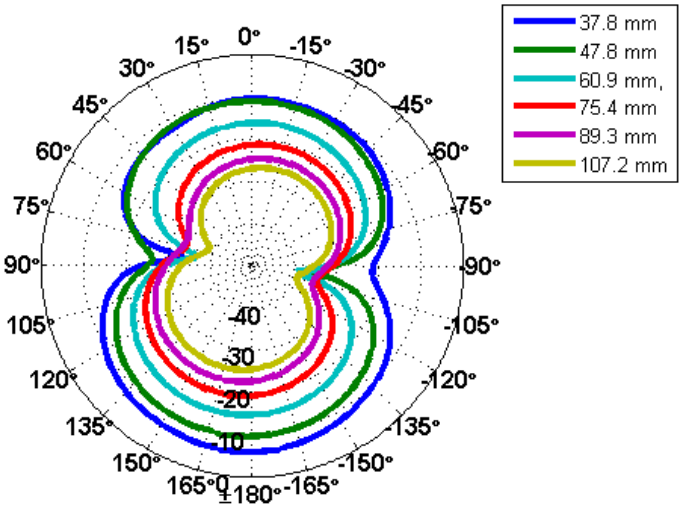


Figure 3.5: Realized gain theta polarization Θ-cut plane at $\Phi = 90°$.

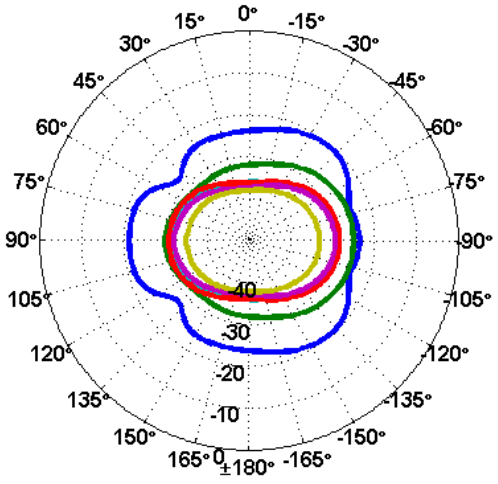


Figure 3.6: Realized gain theta polarization Φ-cut plane at $\Theta = 90°$.

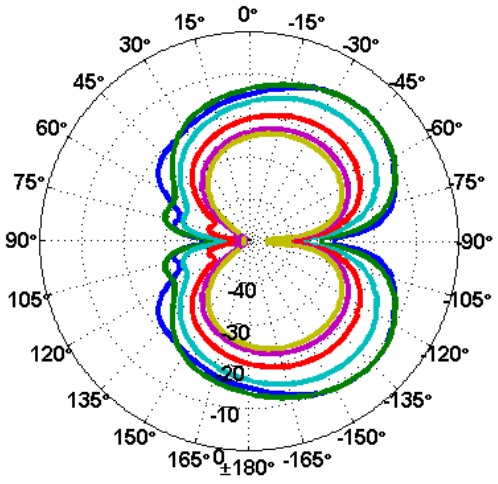


Figure 3.7: Realized gain phi polarization Φ-cut plane at $\Theta = 90°$.

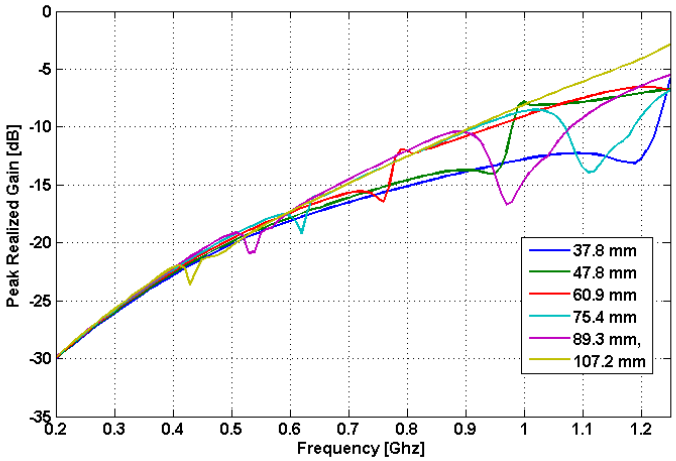


Figure 3.8: Peak realized gain for each structure across frequency. Each curve represents a different arm length.

electrically small. When the disconnect is introduced, the radiation takes on a more ambiguous form.

Some two-dimensional realized gain patterns are plotted in Figures 3.5-3.7 where the cut planes are referenced to the coordinate system laid out in Figure 3.1. There is a null almost directly broadside to the structure in both theta and phi polarizations, but the structure is primarily theta polarized in the YZ-plane. The structure has a more omnidirectional pattern for theta polarization along the XZ-plane and is primarily phi polarized in the XY-plane. Figure 3.8 additionally shows the peak realized gain for each structure. Whereas the total power radiated increases with each resonant arm length, there is no appreciable increase in gain for these same lengths. Instead, the peak realized gain decreases before each dip in VSWR and attains a peak value before peak power radiated of the structure. The peak power radiated actually corresponds to a lower realized gain. This is likely due to the arm resonator behaving more like a transmission-line matching component, such as a shunt stub, rather than an effective radiator itself, or strong coupling from the arm to the rest of the structure prevents field detachment as radiation. Essentially, at the low VSWR the structure accepts more power, but radiates a lower percentage of it, thus the efficiency decreases.

3.3 Isolated Aperture Arms

For more insight on the behavior of the disconnected aperture edge treatment structure, additional study was necessary. It was observed from plotting the surface currents on the conductor containing the edge treatment that negligible amounts of current flow on the inner aperture loops. Removing the aperture loops and isolating the disconnected aperture arms to model a new structure to simulate in HFSS

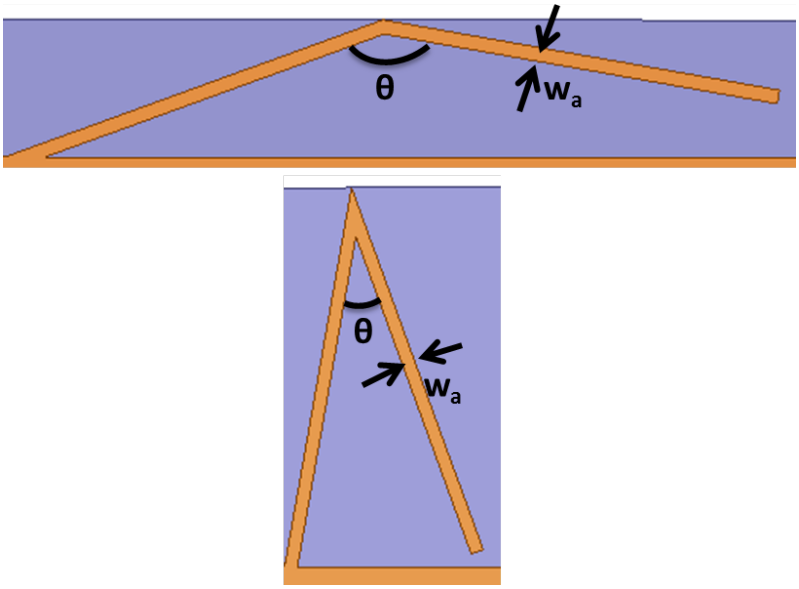
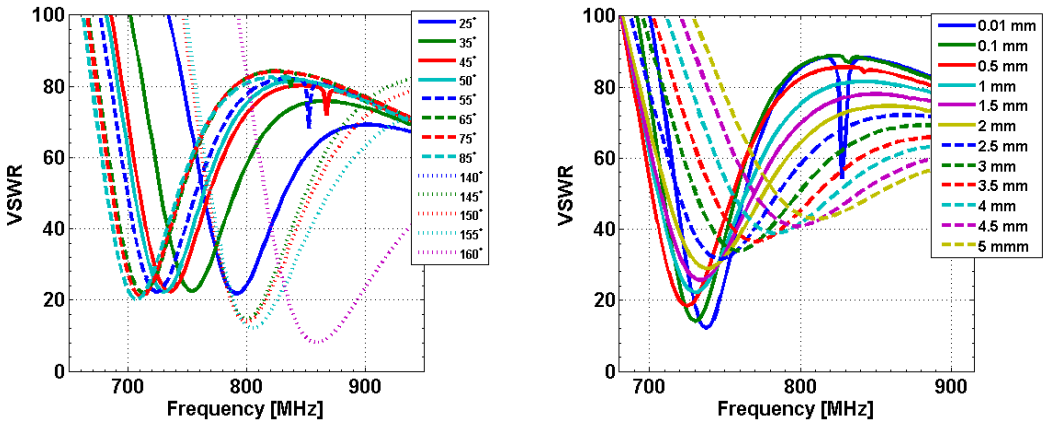


Figure 3.9: Aperture arm structures

should provide some more insight into the behavior of the structure overall.

A structure with a variable aperture arm position and arm width was constructed and analyzed in HFSS and is shown in 3.9. First, the bend of angle θ was varied while the width was kept constant at $1mm$. The bottom structure in Figure 3.9 had arm bend varying at $25°, 35°, 45°, 50°, 55°, 65°, 75°, 85°$, while the top structure in Figure 3.9 had arm bend varying at $140°, 145°, 150°, 155°, 160°$. VSWR of this parametric simulation is shown in Figure 3.10(a). Next, the width of the arm w_a was varied while the angle bend θ was kept constant at $50°$. VSWR of this parametric simulation is shown in Figure 3.10(b). The overall length of the arm was kept constant for all cases.

From these results, it can be seen that varying the angle of the arm bend will shift the resonance of the structure. As the arm bend angle increases, the coupling between the lengths of the arms and the parallel plate feeding structure likely decreases, causing the resonance to shift down in frequency; but at the largest arm bend angles, the entirety of the arm is closer to the parallel plate feed structure, ef-



(a) (b)

Figure 3.10: 3.10(a): VSWR when varying bend angle θ, and 3.10(b): VSWR when varying arm width w_a

fectively increasing the coupling overall and shifting the resonance up in frequency. Varying the arm width has more effect on the bandwidth of the structure as shown by the widening of VSWR as the arm width increases. This occurs because increasing the arm width effectively increases the overall electrical size of the arm, but consequently increases the impedance mismatch.

3.4 Transmission Line Model of Aperture Discontinuity

The sections of the structure containing the apertures and the disconnected aperture arms closely resemble characteristics of microstrip transmission line. The expected mechanism for radiation of this structure is from the disconnected aperture arms acting as bent microstrip monopoles which resonate when they approach a third of a wavelength. Since the sections containing the apertures experience very little current flow, they not believed to contribute much to radiation.

A transmission line model for the full structure containing the triangular apertures and disconnected aperture arms was developed and compared to HFSS so the

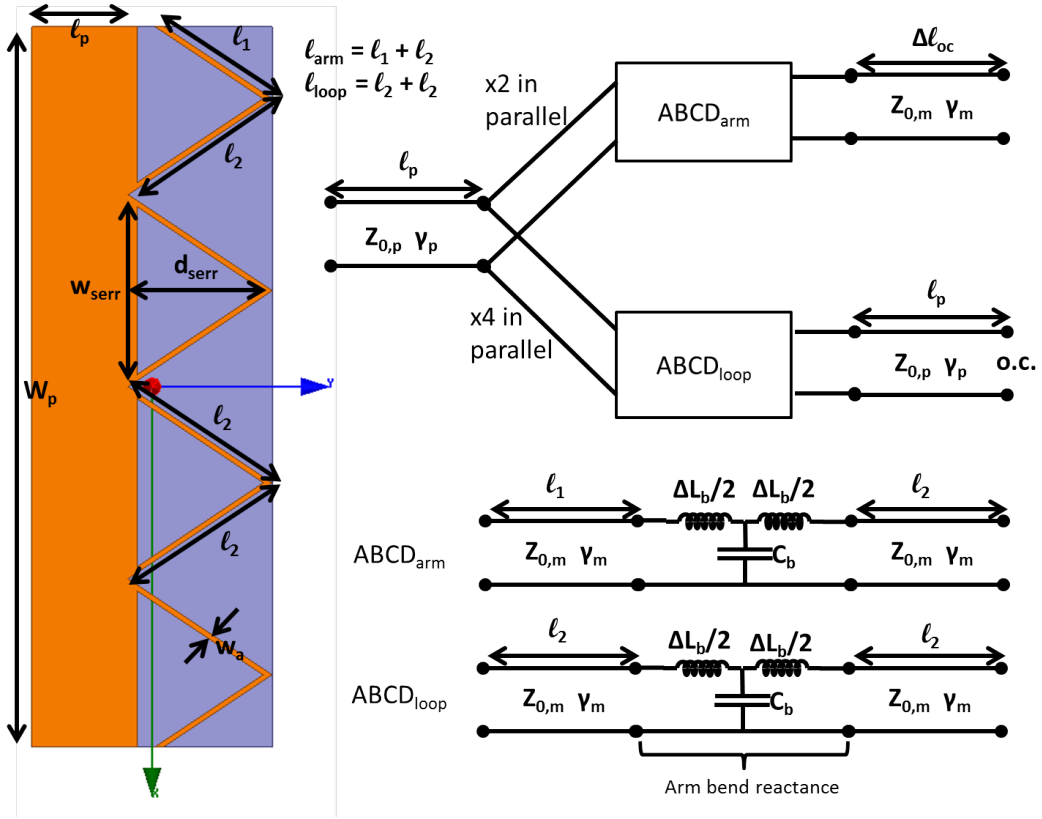


Figure 3.11: Transmission-line model for the edge treatment structure containing apertures and the radiating arms.

impedance behavior of the individual components can be characterized. Each disconnected arm is modeled as a length of microstrip line containing a right-angle bend [12] and terminated in an open-ended microstrip discontinuity which is modeled as a delta length of open circuited microstrip transmission line [13]. Each aperture loop section is modeled as a length of microstrip line containing a right-angle bend and terminated in a length of open-circuited parallel-plate transmission line which mimics the line looping back onto itself.

The current model is shown in Figure 3.11. The model shows a length of parallel-plate transmission line which branches off into two parallel lengths of the microstrip arm sections and four parallel lengths of microstrip loop sections to ac-

W_p	ℓ_p	w_{serr}	d_{serr}	ℓ_1	ℓ_2	w_a
150	40.625	40	10	16.77	20	0.56
150	31.25	40	20	21.21	25	0.89
150	21.875	40	30	27.04	32	1.05
150	12.5	40	40	33.54	40	1.12

Table 3.1: Table of disconnected aperture structure dimensions used in HFSS simulation. All dimension are in millimeters.

count for all possible directions for current flow. ABCD parameters are utilized for each section of microstrip because once the full cascaded sections of ABCD matrices are found, the input impedance for each section of line is computed to find the total input impedance that is in parallel to the parallel-plate transmission line. Thus, the total input impedance of the structure is readily computed afterwards.

The result of the transmission line model when compared to an HFSS simulation is shown in Figure 3.12. The structure was simulated at values shown in Table 3.1. There is reasonable agreement between the model and HFSS for the first series and parallel resonances aside from the magnitude differences at the resonances and at the lower end of frequency sweep.The model in its approximate stages is also mostly accurate for only a TEM case. Higher order modes start becoming excited within the parallel-plate around 1 GHz, causing a fall-off of accuracy for the model beyond 1 GHz. Additional coupling and parasitic effects still need to be modeled for the TEM because the model assumes a 90° arm bend, when the arm bend angle actually varies form a right angle as result of the parametrization of the HFSS model's dimensions.

The transmission model neglects conductor losses since it is comparing to an HFSS simulation where the top and bottom plates are modeled as perfect electric conductors. Dielectric losses are included which account for the complex propaga-

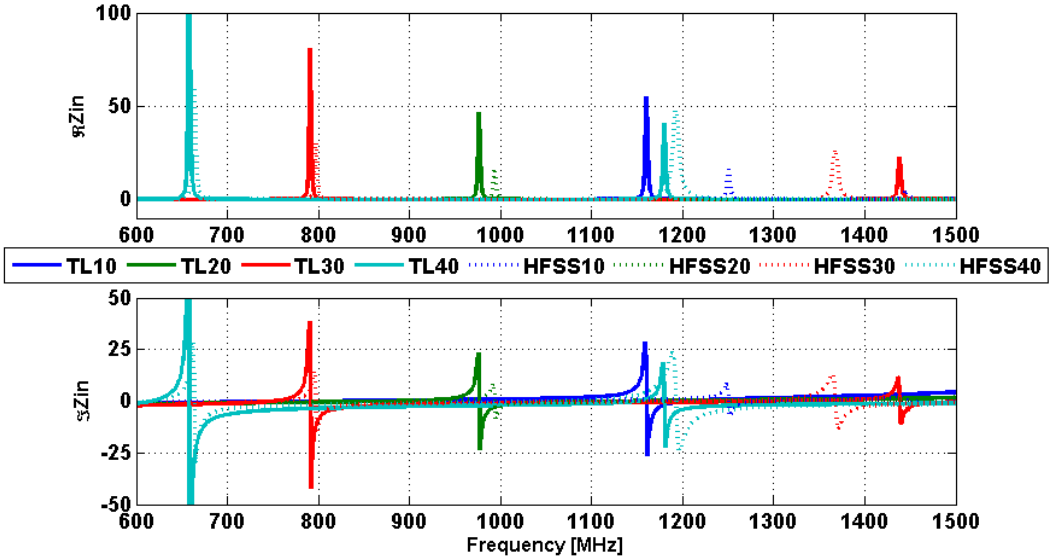


Figure 3.12: Input impedance of transmission-line model for the edge treatment structure containing apertures and the radiating arms. The curves are designated as TL## or HFSS## in which the ## corresponds to a serration depth mentioned in Table 3.1.

tion constant being modeled into each length of line. Further discrepancies between the model and simulation may be due to the absence of radiation loss being modeled into the disconnected aperture arms.

3.5 Conclusions

A structural error in one of the HFSS models from the study in Chapter 2 was identified. Inspection of the model of the triangular aperture serration edge treatment revealed a break in the continuity of the aperture loops located at the edges of the structure. This structure possesses an electrically small impedance match that occurred at a smaller electrical size than any of the other edge treatments in the parametric study. A study on this result revealed that the disconnected aperture becomes a resonating arm that essentially acts as an impedance matching element taking the

form of a open-ended microstrip transmission line. This impedance match also results in a greater total power radiated by the structure. Although this presents desirable performance, the coupling and radiation mechanisms of the aperture arm are so that they do not increase the overall radiation efficiency of the structure which results in a lower realized gain.

A transmission line model was derived based on the edge treatment structure used in HFSS simulations. The model treats the aperture loops and disconnected arms and microstrip transmission line containing a right angle bend. The aperture loops terminate in open-ended parallel plate waveguide while the disconnected arms terminate in a delta length of open circuited transmission line that accounts for the open-ended discontinuity fringing fields. Only dielectric losses are included in the model - conductor losses are ignored because the simulation model conductors are modeled as PEC. The model is currently a rough estimation of the current setup, thus it still needs to take into account many parasitics and coupling effects that arise from the disconnected arm and aperture loops. Additionally, radiation loss needs to be included in the model to account for the radiation mechanism of the structure.

Chapter 4

Application to Large Ground Plane

4.1 Introduction

An antenna in the presence of a ground plane will couple some of its energy into the ground plane where it experiences an interaction that is highly dependent on the way the antenna is set up over the ground plane and how the antenna radiates. One can look no further than to image theory for a simple example. This example involves a vertically oriented current source radiating vertically polarized fields above a ground plane that is flat, perfectly conducting, and infinite in extent. The radiated fields impinge on the ground plane and then reflect in a matter that is dependent on the angle of incidence which can be modeled as fields radiated from a virtual source below the ground plane. The reflected fields may add or cancel with the radiated fields that do not reach the ground plane and alter the radiation pattern from if the current source was radiating into freespace. Infinite ground planes do not exist in practice, but they provide reasonable approximations for finite, but electrically large, ground planes; also the concept can be extended to explain other phenomena where an antenna radiates onto a ground plane.

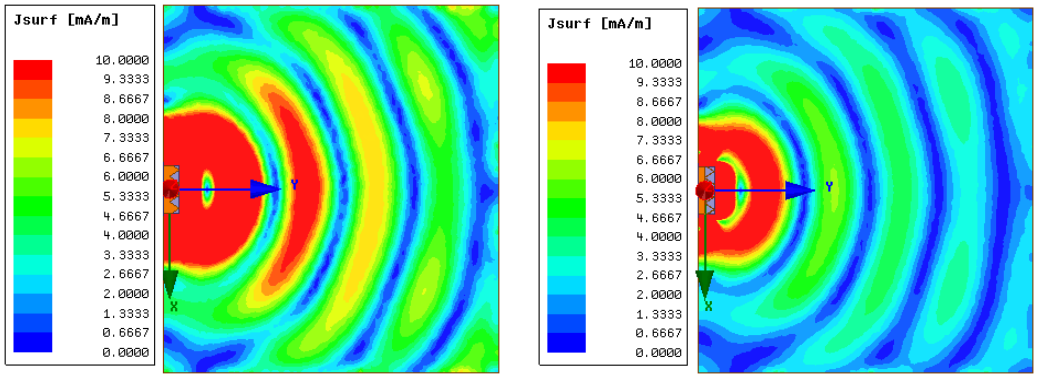
For ground planes that are finite in extent, several mechanisms come into play for describing the interaction of incident fields with the ground plane. Fields ra-

diated from an antenna structure onto a ground plane will scatter from the ground plane in a manner reminiscent of image theory, but also fields that reach the edges of the ground plane will diffract off the edges. Both scattered and diffracted fields will interact with the radiated fields that will alter the overall pattern. Radiated fields may also induce currents onto the ground plane that affect the overall radiation to the degree of how strong those currents are and whether the induced currents line up with inherently supported current modes of the ground plane (i.e. from Characteristic Mode Theory).

This chapter contains an examination of two edge treatment variations when put in the condition to radiate onto a ground plane. Radiation and coupling mechanisms of these edge treatments are theorized, but not definitively given - a task which will be completed in future work. A placement insensitive antenna containing the triangular serration edge treatment is designed as the basis for comparison of relative performances for other edge treatment types when included in the antenna design. Performance is analyzed for each edge treatment when the antenna contains just a truncated conductor backing and when the antenna is placed over a larger ground plane. Additionally, some measures of current induction capabilities for each antenna on the larger ground plane are examined.

4.2 Edge Treatments on Ground Plane

Work was done on evaluating the capabilities of edge treatment structures in inducing ground plane currents. The goal is to induce a high enough current intensity so that the ground plane itself contributes to the radiation mechanism of the structure when it is placed over a ground plane. The steps needed to be taken for this study includes understanding how currents might be induced on a ground plane and which



(a) (b)

Figure 4.1: (a): Currents induced on ground plane from the triangular serration edge treatment; (b) Currents induced on a ground plane from the triangular aperture edge treatment containing disconnected apertures on the ends.

edge treatment is capable of inducing the highest surface current intensity.

Figure 4.1 shows an HFSS simulation result for surface current intensity on a ground plane when the structures, one containing electrically small triangular serrations (4.1(a)) and the other containing electrically small triangular apertures with the disconnected aperture arms at the ends (4.1(b)), are placed at the center of one of the edges of the ground plane. The structure is fed at 750 MHz which pertains to a wavelength of 400 mm. The ground plane is modeled with finite copper conductivity and is a square with length and width both at 1 meter. The ground plane is thus 2.5λ long electrically at 750 MHz. When the power put into the structure is 1 Watt, the amount of current induced from the radiated fields is on the order of milliamps and attenuates the further the fields are from the structure.

The low magnitude of the current induction is due to each edge treatment being electrically small, and thus not being able to radiate a very high percentage of the input power. Although, it is clear from Figure 4.1 that the triangular serration edge treatment induces more currents than the triangular apertures edge treatment. This is an interesting result considering, from Figure 4.2(a), that the triangular aper-

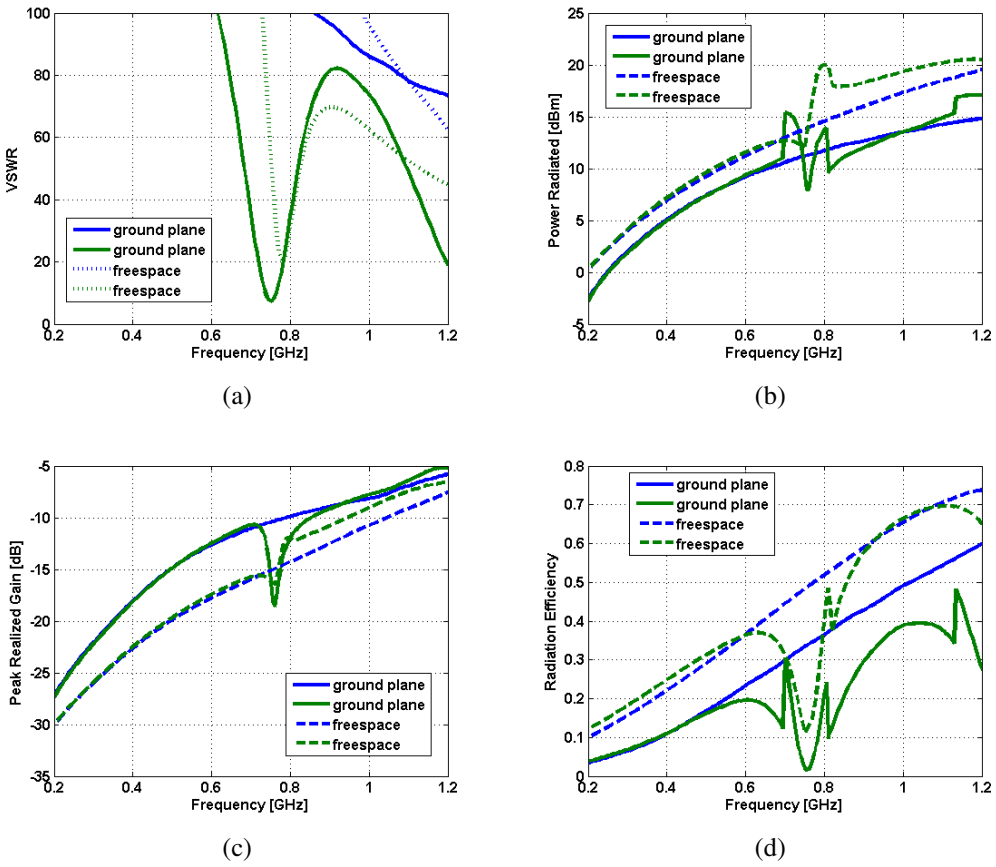


Figure 4.2: Plots comparing the performance of the triangular serration edge treatments (blue curves) and the triangular aperture edge treatments (green curves) when radiating onto a ground plane vs into freespace where (a): VSWR; (b) power radiated in dBm; (c) peak realized gain in dB; (d) radiation efficiency. The freespace curves pertain to when the edge treatment is simulated with the truncated conductor backing, and the ground plane curves pertain to the extended ground plane case shown in Figure 4.1.

ture edge treatment experiences a greater impedance match than the triangular serration edge treatment at 750 MHz when either placed onto an extended ground plane or containing the truncated conductor backing. Furthermore, From Figures 4.2(b), 4.2(c), and 4.2(d), the radiation performance of the triangular aperture edge treatment degrades at 750 MHz compared to its performance when the conductor backing is truncated. The triangular aperture edge treatment radiates less power compared to the freespace case as evident by the incredibly large decrease in radiation efficiency. Alternatively, the peak realized gain for both edge treatments is, on average, greater when radiating onto a ground plane vs just into freespace. The higher gain is likely due to the reflections off the ground plane and diffraction at its edges, and not directly related to the efficiency of each structure when compared to radiating in freespace.

Referring to the realized gain patterns for both edge treatments when they radiate into freespace, the triangular serration edge treatment has a larger broadside gain for the theta polarization than the triangular aperture edge treatment containing disconnected aperture arms at 750 MHz - the triangular aperture edge treatment with disconnected aperture arms effectively contains broadside nulls. The triangular aperture edge treatment containing disconnected aperture arms instead radiates mostly in the z-direction. The freespace radiation behavior is one indication on the amount of coupling that will take place once the edge treatment radiates onto a ground plane. This shows that the choice of edge treatment to be used on a ground plane is more critical, that careful consideration should be taken when trying to determine the best edge treatment for exciting currents on a ground plane. Also, the ground plane has an effect on the edge treatment performance - aside from what just the simulations from Chapter 2 have shown.

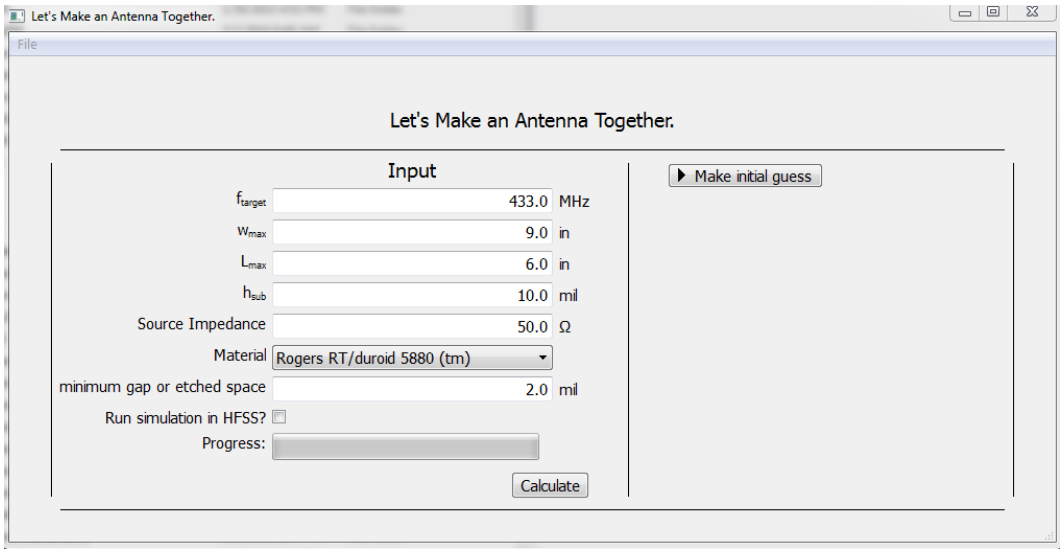


Figure 4.3: Antenna design GUI for conductor-backed spiral inductor loaded slot antenna containing serrated edges.

4.3 Antenna Design

Since one of the original goals of the edge treatment investigation of Chapter 2 was to determine the best edge treatment for inclusion into the design of a placement insensitive antenna, such an antenna is to be used for comparison study of edge treatments in their current induction capabilities on a ground plane. Redefining the antenna: the placement insensitive antenna is a dielectrically backed electrically small rectangular slot antenna that is end-loaded with spiral slot inductors. Two edges, of the ground plane that contains the slot, contain the triangular serration edge treatment because the edge treatment allows parallel plate waveguide modes, excited from aperture coupling, to escape from between the slot ground plane and the conductor backing that the antenna is placed on. If these modes don't radiate away, their energy will reflect back and couple into the slot which creates and undesirable reactive loading effect that de-tunes the antenna.

Given some of the features of the aforementioned antenna, it is inherently com-

plex in its design. A computer program and design manual [14], created by students, faculty, and engineers at the University of Oklahoma, circumvents some of the complexities of designing the antenna by allowing the designer to input design parameters (e.g. operating frequency substrate type and height) into a graphical user interface (GUI), shown in Figure 4.3, and letting the program design the antenna through an automated iterative procedure. The iterative procedure includes using design formulas to optimize the design in MATLAB and simulating the resulting design in HFSS. The procedure is repeated as needed until the antenna operates at the desired frequency based on the input criterion provided by the user. After a preliminary design is provided by the program, manual tweaking of some of the antenna's dimensions is sometimes necessary to shift the resonant impedance match to the desired operating frequency. It is pertinent to note that the antenna is designed with a truncated conductor backing that is the same length and width as the substrate because it is important in determining serration dimensions that will fit the input parameter criterion.

An antenna containing the triangular serration edge treatment was to be the base model to compare the other edge treatments to because it is the original edge treatment used in the antenna design and is the only edge treatment included in the design formulas. The base antenna was designed to operate at 433 MHz on a 10 mil Rogers RT/Duroid 5880 substrate. The final design of the antenna is shown as an HFSS model in Figure 4.4. Some of the key dimensions of the antenna are listed in Table 4.1.

$w_{serr}(mm)$	$d_{serr}(mm)$	$L(in.)$	$W(in.)$
7.62	90	6	9

Table 4.1: Key dimensions of antenna from Figure 4.4.

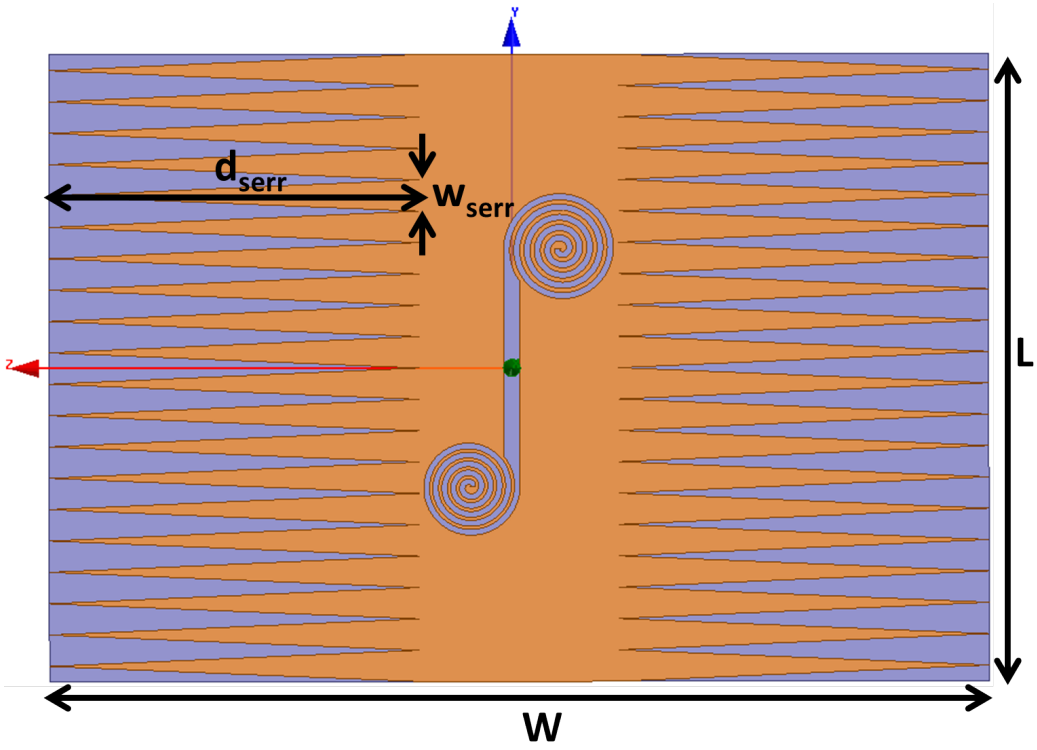


Figure 4.4: HFSS model for antenna containing triangular serrations given by the antenna design program.

To study the effect that each of the edge treatments have on the full antenna structure and also in their current inducing capabilities, the final dimensions of the antenna and triangular serration edge treatments determined from the program and manual tweaking are to be kept constant while the type of edge treatment is changed. The same edge treatments studied in Chapter 2 are to be used as edge treatments for the antenna, with the exception of the triangular serration edge treatments containing the circle and diamond apertures. Additionally, the serration edge treatment with triangular apertures that resulted in a disconnected aperture arm in the model is not included in the study due to the reason that it was not originally intended to be used for comparison - although future work may include this structure. Lastly, the half circle edge treatment is slightly altered into an ellipse shape for the

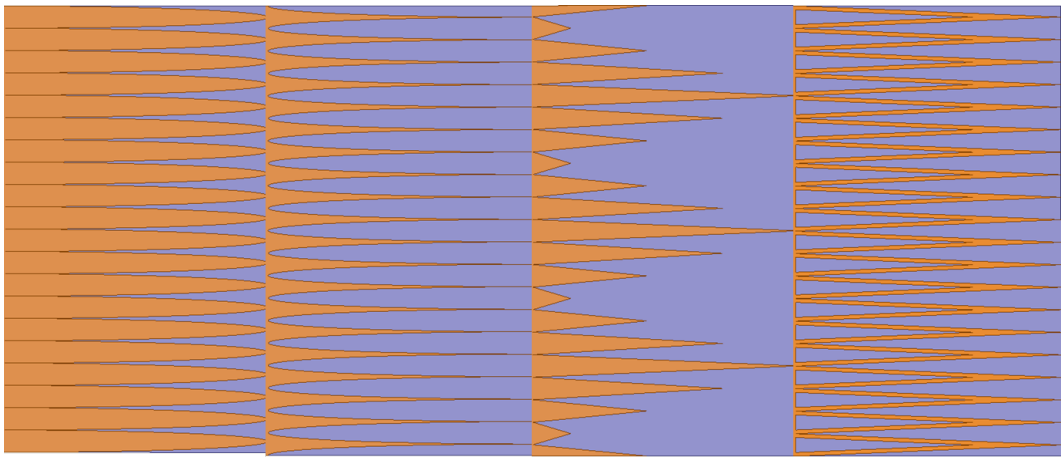


Figure 4.5: HFSS models of each additional edge treatment structure included in the antenna. Left to right: ellipse, curved, subtriangular, triangular apertures.

sake of keeping relative dimensions constant. The inclusion of each additional edge treatment, in place of the triangular serrations, on the antenna that was designed at 433 MHz is shown in Figure 4.5.

4.4 Simulated Antenna Performance Off and On Large Ground Plane

Each antenna was simulated in HFSS with the truncated conductor backing, and again with the conductor backing extended at dimensions of 2 meters by 2 meters ($\sim 6.6'$ by $6.6'$) which simulates the antenna being on a large ground plane. The slot ground plane and conductor backing were modeled with finite thickness of 17.5 micrometers and conductivity of copper. The substrate is a 10 mil Rogers RT/Duroid 5880 with a relative permittivity of 2.2. The antenna is being excited at the center of the slot with a lumped element port of 50 Ohm characteristic impedance.

The input impedance of each antenna with the truncated conductor backing is shown in Figure 4.6. It is clear that the type of edge treatment being used by the

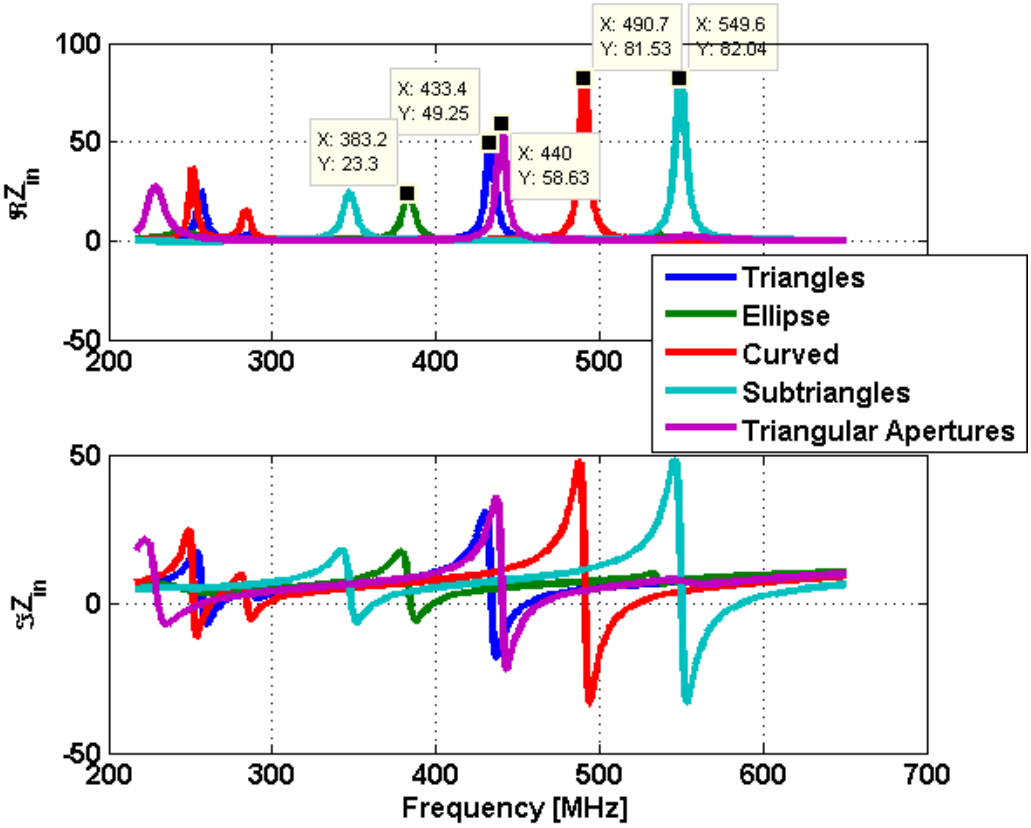


Figure 4.6: Input impedance for each antenna containing a different edge treatment, with each curve named after which edge treatment the antenna contains.

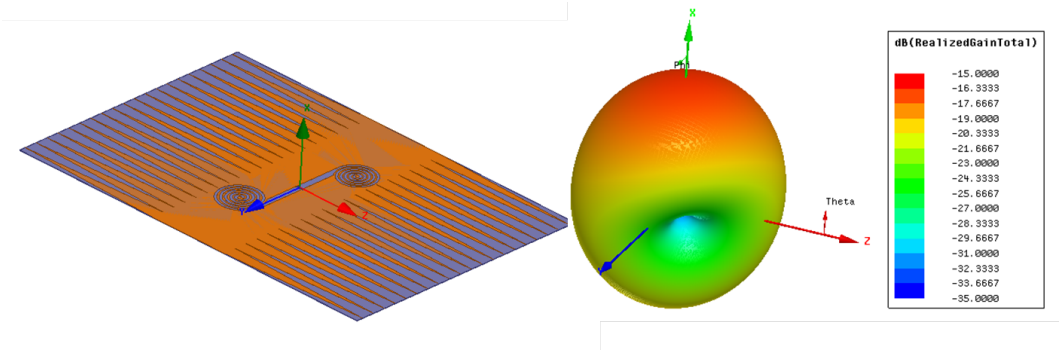


Figure 4.7: Antenna containing triangular serration edge treatment next to its 3-dimensional realized gain pattern.

antenna has an effect on its behavior. The edge treatments are part of what dictate the operating frequency of the antenna. The ellipse edge treatment tunes the impedance down in frequency. This is due to its larger and more curved geometry which makes the edge treatment electrically larger overall. This presents the possibility of shrinking the overall dimensions of the antenna which is useful for miniaturization purposes. Both the curved and ellipse edge treatments tune the impedance up in frequency. Their smaller relative electrical sizes are likely the cause for this. Adding an aperture to the edge treatment shows to provide only minor changes to the operating frequency impedance, which is consistent with the data that the parametric investigation provided in Chapter 2. The addition of the edge treatment on the antenna obfuscates some of the behavioral properties of the edge treatments due to the nature of the antenna being electrically small. The electrical size of the antenna inherently causes its operating bandwidth to be very small.

To gain an understanding of how each antenna would induce currents on the larger ground plane, it is important to provide some context on how they radiate. The realized gain pattern for the antenna containing the triangular serration edge treatment relative to its orientation on an axes is shown in Figure 4.7. The antenna possesses a ”dipole-like” pattern. Most of the energy coupling into the parallel-

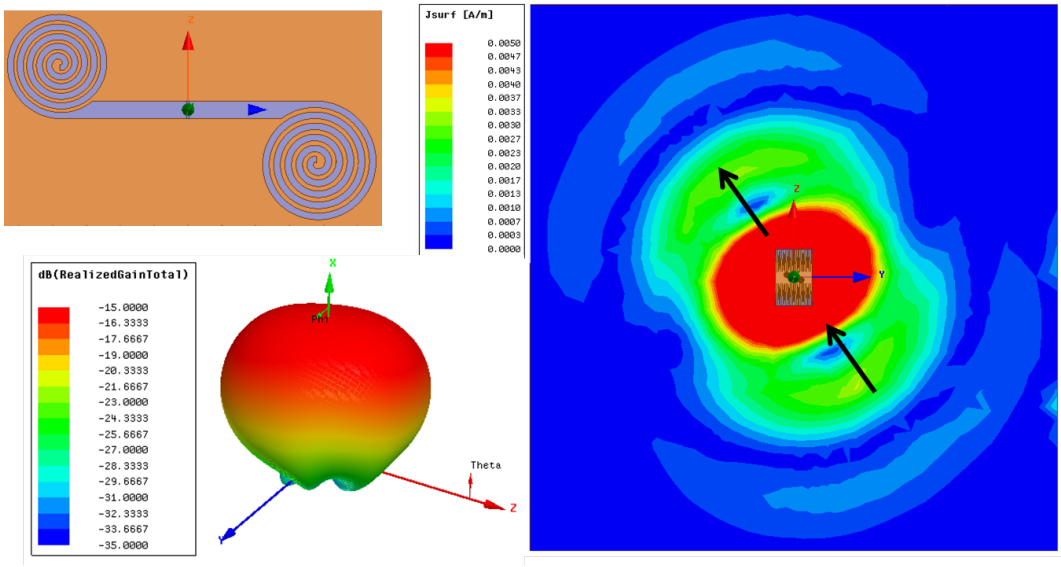


Figure 4.8: Antenna containing triangular serration edge treatment placed on larger ground plane. (Top left) Orientation of the slot on the ground plane; (Bottom left) Realized gain pattern for the antenna on the larger ground plane; (Right) Induced current magnitude on the ground plane with arrows indicating direction of current flow.

plate modes occurs at the spiral inductors. Thus, most of the fields on the edge treatment are stored outward from the spirals in the planes parallel to the depth of the serrations. This causes the polarization of the radiated fields to be skewed off axis from the polarization of the slot fields. The radiation pattern is the same for the other antennas, but the skewness angle is slightly different for each edge treatment, but along the same direction. For each antenna, there is also negligible change to the input impedance at the resonant operating frequency of the antenna when the conductor backing is extended in size to the larger ground plane lengths.

Figure 4.8 shows the realized gain pattern and induced current magnitude and direction of the antenna containing the triangular serration edge treatment when radiating over the large ground plane. The realized gain of the antenna is shown to increase broadside to the antenna with minimized back-plane radiation. The direc-

		Truncated GP		Larger GP	
Edge Treatment	d_{serr}/λ_r	η_{eff}	Gain$_R$ (dB)	η_{eff}	Gain$_R$ (dB)
Triangular	0.19	0.72%	-17.24	0.62%	-15.00
Ellipse	0.17	0.34%	-22.51	0.39%	-18.28
Curved	0.24	1.77%	-12.65	1.04%	-13.14
Subtriangular	0.24	1.93%	-12.31	0.93%	-13.52
Apertures	0.20	N/A	N/A	N/A	N/A

Table 4.2: Radiation efficiencies and peak realized gain for each edge treatment's operating electrical size on the antenna. Data is obtained from HFSS for each antenna with truncated conductor backing and extended ground plane backing. No data was obtained of the antenna with triangular apertures edge treatment. GP stands for ground plane.

tion of the induced currents are also consistent with the polarization of the radiation, showing that the antenna induces currents off axis from the polarization of the slot fields. Each antenna, when simulated on the larger ground plane, induces currents in the same fashion as the antenna with the triangular serration edge treatment.

The salient features of the radiation characteristics for each antenna relative to their edge treatment's depth electrical length are summarized in Table 4.2. From the data, the efficiency and realized gain for the antenna containing the ellipse serration edge treatments experiences an increase; the efficiency decreases while the realized gain increases for the antenna containing the triangular serration edge treatment; and the efficiency and realized gain for the antennas containing the curved and subtriangular serration edge treatments experience a decrease. No simulated radiation data is available for the antenna containing the triangular aperture edge treatment due to convergence issues with HFSS. The electrical sizes of the antennas and ground plane at the differing operating frequencies, the degree of impedance mismatch from 50 Ohms for the antennas that aren't matched, the orientation of each antenna on the ground plane, and in the same reign as the impedance mis-

match - the amount of current induced on the ground plane are all likely factors responsible for the inconsistent trends of the efficiencies and realized gain for each antenna. This shows that each of those factors are important considerations to address when determining which edge treatment would possess the highest gain and efficiency increase.

4.5 Conclusions

An antenna radiating out on a ground plane is capable of inducing currents on the ground plane that can have an effect on the overall radiation behavior of the antenna. The ability of antenna edge treatments in inducing currents on a ground plane, so the ground plane can either aid in the radiation or become the radiator itself, was examined. The magnitude of current that is induced on a ground plane is not independent of edge treatment type. How an edge treatment radiates in a freespace condition can provide some inference into how the currents may be induced, but the addition of a large ground plane to an edge treatment has the potential to significantly alter the radiation mechanism of the edge treatment. Impedance match and efficiency, edge treatment shape and electrical size, position on the ground plane, and size of ground plane can all have an effect on the total radiation behavior.

Five of the edge treatments from the parametric investigation in Chapter 2 were included in the antenna design of the placement insensitive antenna to determine their performance in the full system. It was shown that the type of edge treatment included on the antenna has an effect on the operating frequency and impedance magnitude for the antenna. The ellipse serration shows the most potential for size reduction, but more study is needed on changing its electrical size to determine its performance. The study was also extended to placing the antenna on a larger

ground plane to observe the effects of each edge treatment on inducing currents on a ground plane and the resulting radiation behavior. The ellipse serration edge treatment antenna experienced the highest gain increase, while the other edge treatments experience either decrease in gain, efficiency, or both. Electrical size of all aspects of the antenna and the ground plane have an effect on the overall coupling and radiation, but the exact coupling mechanism for the edge treatments into the ground plane has not yet been determined and is the subject of future work. Additionally, future work of examination of each edge treatment when all are tuned to the same operating frequency may provide more insight into the behavior of each antenna and its edge treatment type.

Chapter 5

Measurements

5.1 Introduction

Each antenna that was simulated in Chapter 4 was fabricated and tested to verify the theoretical results. Scattering parameters were measured on a network analyzer, while antenna radiation patterns were obtained by taking far-field measurements inside an anechoic chamber.

This chapter will present the fabricated antennas, as well as the ground plane that was constructed for current induction by the antennas. An additional antenna pattern calibration procedure is discussed which allows realized gain of the antennas under test to be extracted. A discussion on the application of characteristic mode theory for using the modal currents of the ground plane to aid in radiation is included, followed by graphic depictions of modal currents determined to be useful for the designed antennas. Finally, the aforementioned measurements are shown along with a discussion of the results and potential future direction that can be taken.

5.2 Constructed Entities

10 mil Rogers RT/Duroid 5880 substrates with half ounce (17.5 μm) copper cladding were procured for antenna fabrication so as to match the substrates used in the simulation models. One side of each of the the boards was etched, according to their respective designs, using standard photolithography techniques. The reverse side of each board contains one small rectangular aperture at the center of the conductor that indicates where the probe feed that excites the slot should be placed. The resulting fabricated antennas are shown in Figures 5.1-5.5.

Each antenna is fed via a probe feed at the center of the slot, from the conductor-backing side, with 50 Ohm semi-rigid coaxial cable transmission line. Since the slot antenna is a balanced structure, and the coaxial cable is not, a balun was necessary to include between the antenna terminals and feed transmission line. A quarter-wave bazooka balun was chosen due to its high common mode current rejection ability. The bazooka balun possesses only about 10% bandwidth due to the nature of its operation, so a different bazooka balun was constructed for each antenna, and whose length corresponds to a quarter-wavelength of its antenna's operating frequency. One of the baluns can be seen in Figure 5.6, behind the front face of the antenna.

Center-fed half-wave dipoles are utilized in calibrating the antenna pattern measurement values obtained inside the anechoic chamber. Five dipoles were constructed, each one resonating at a half-wavelength at a corresponding operating frequency of the five placement insensitive slot antennas under test. Copper wire is used as the arms of the dipole, and the dipole terminals are also fed by 50 Ohm semi-rigid coaxial cable with a quarter-wave bazooka balun in between the dipole arms and feed line. One of these calibration dipoles is shown in Figure 5.7.

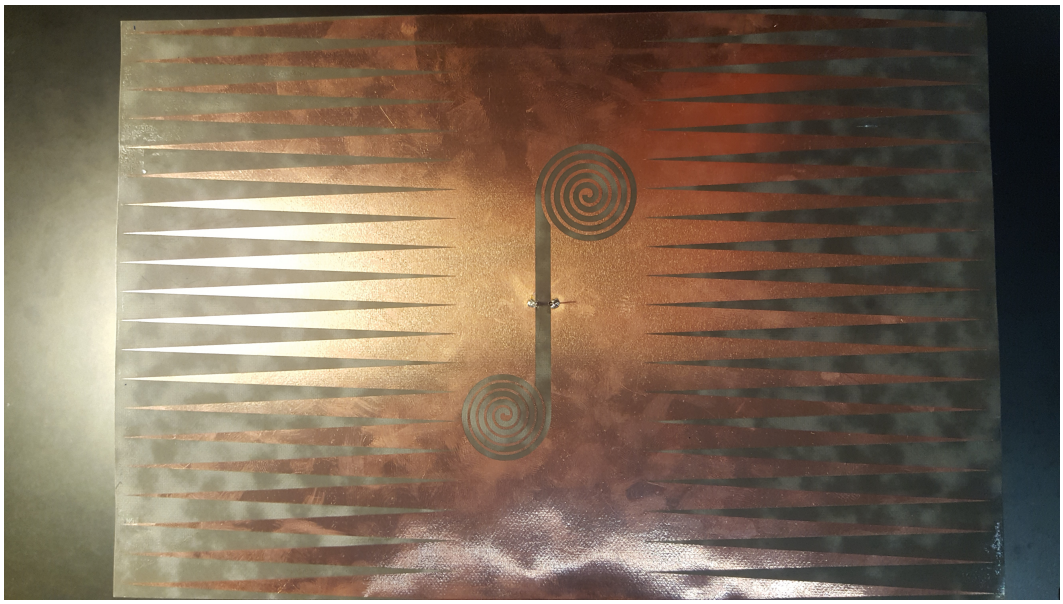


Figure 5.1: Fabricated conductor-backed slot antenna containing the triangular serration edge treatment.



Figure 5.2: Fabricated conductor-backed slot antenna containing the ellipse serration edge treatment.



Figure 5.3: Fabricated conductor-backed slot antenna containing the curved serration edge treatment.

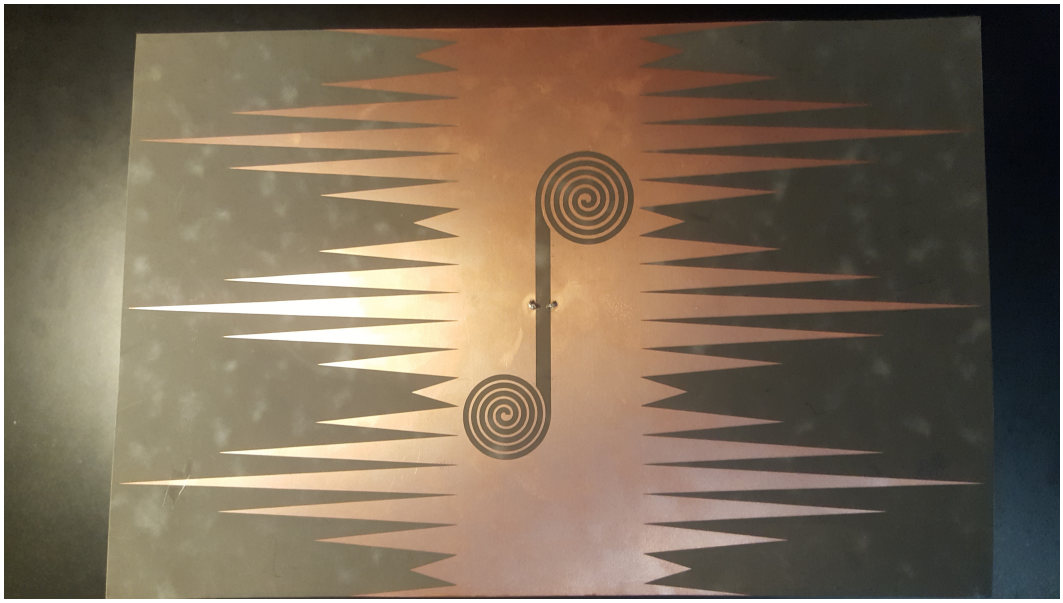


Figure 5.4: Fabricated conductor-backed slot antenna containing the subtriangular serration edge treatment.

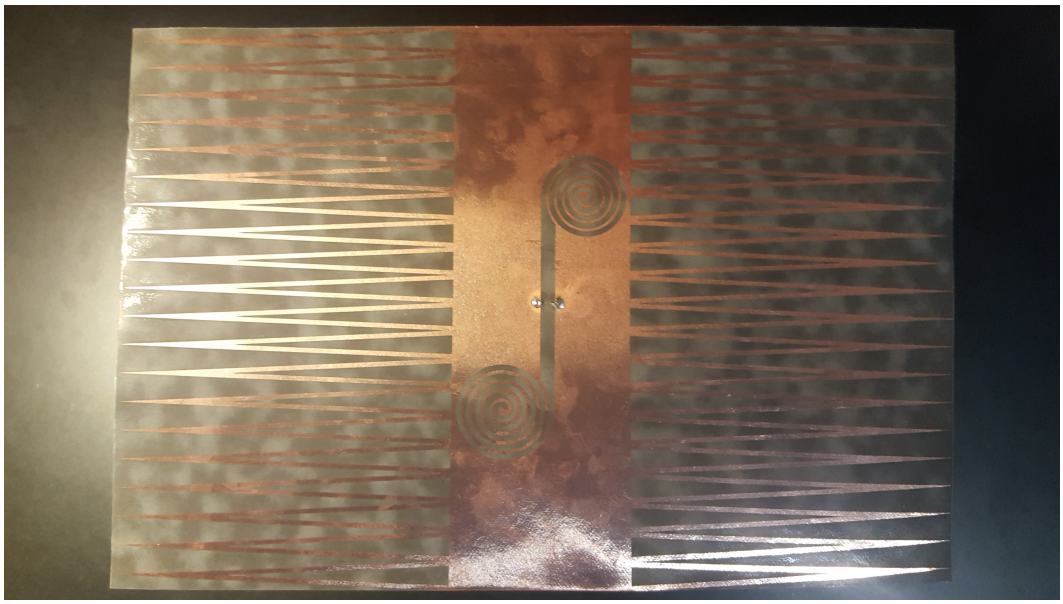


Figure 5.5: Fabricated conductor-backed slot antenna containing the triangular apertures serration edge treatment.

The ground plane constructed for the comparison study is a sixty-four sq-ft square made of copper foil laid out on cardboard, that contains a wooden frame and mounting bracket. One-inch by two-inch by eight-foot wooden boards were used to construct the frame with metal wood-screws used to secure the wood against each other and to secure the cardboard square to the frame. Spray adhesive was used to coat the cardboard square before attaching the copper foil. The copper foil came wound on 6 inch wide rolls. Strips of the copper foil were stretched across one of the dimensions of the cardboard square and copper tape used to ensure electrical continuity across the area of the copper. A wooden mounting bracket was then constructed so the ground plane may be attached to a pedestal mount for the AUT vertical positioner of the anechoic chamber. The front and back of this constructed ground plane is shown in Figure 5.8, where the images also showcase the ground plane mounted inside the chamber.

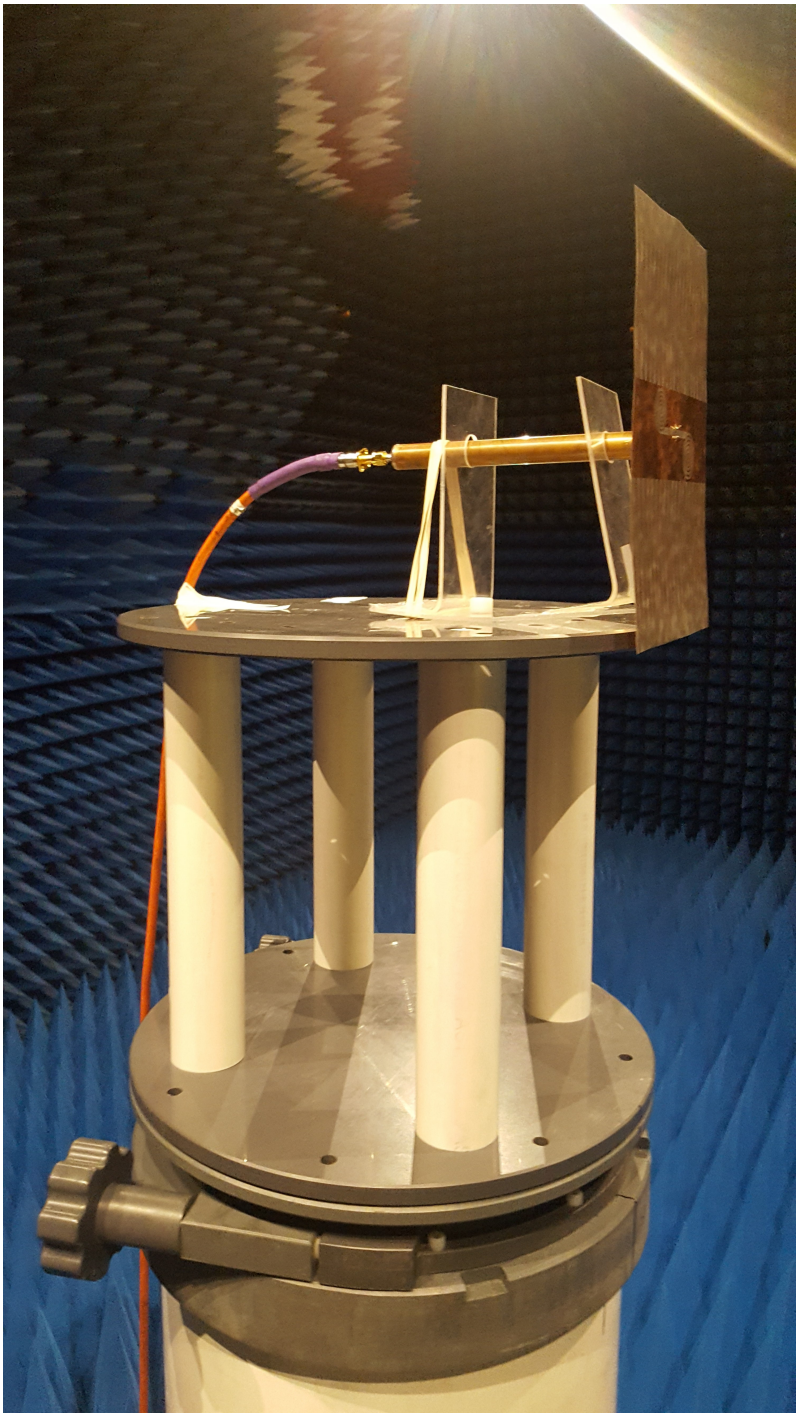


Figure 5.6: The conductor-backed antenna containing the triangular aperture serrations mounted in the anechoic chamber. Feed structure contains quarter-wave bazooka balun.

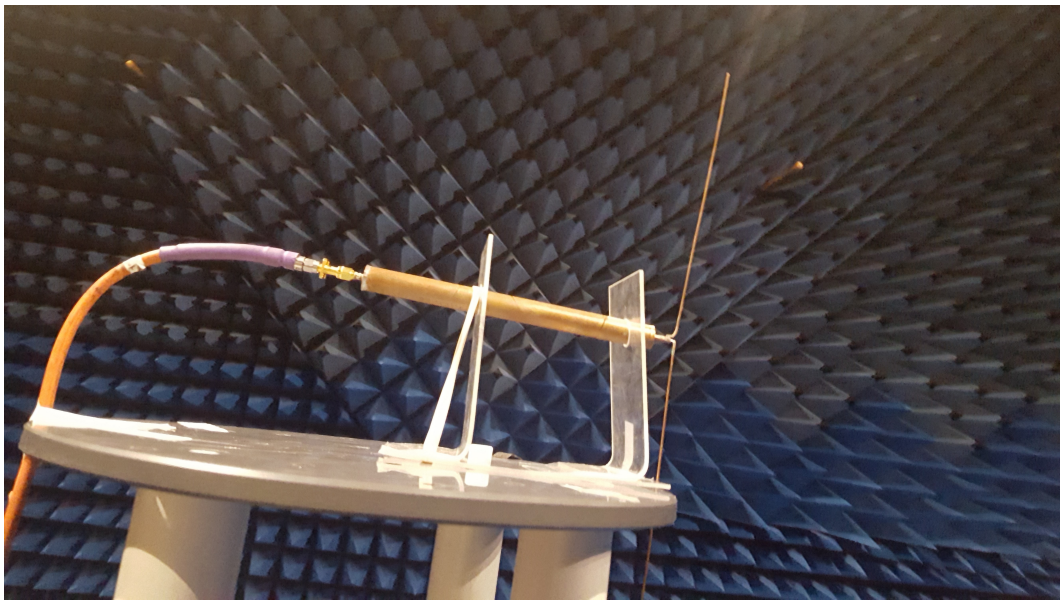


Figure 5.7: Calibration dipole at the operating frequency of the antenna containing the triangular serrations mounted in the anechoic chamber.

5.3 Characteristic Mode Analysis

The theory of characteristic modes of conducting bodies was invoked in this study. Characteristic modes provide insight into radiation and scattering properties of conductors of arbitrary shape by computing current distributions that are inherently supported by the conductor along with the relative modal weight that each current distribution possesses. This becomes useful when trying to determine what parts of the conductor should be excited with what kind of current so as to achieve a desired type of radiation from the conductor.

For antennas, characteristic mode theory can help determine optimal antenna placement on a metallic structure. If the radiation characteristics of the antenna, alone, are known, then this knowledge can be exploited to place the antenna in a spot that lines up with a known current distribution of high modal weighting. This, in turn, allows the antenna to radiate as intended, rather than potentially suppressing



(a) (b)

Figure 5.8: The $8'x8'$ ground plane mounted in the anechoic chamber.

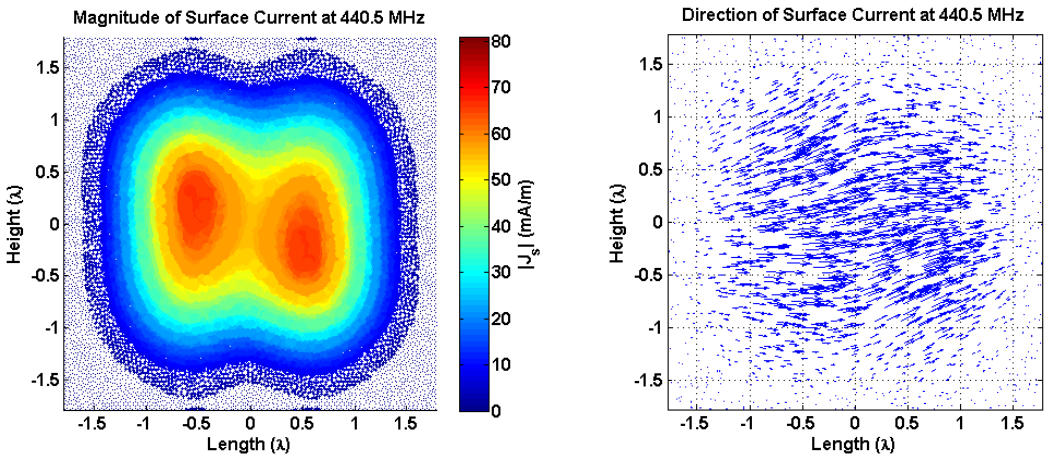
the radiation.

This can also be similarly extended to proper placement of electrically small antennas. Since an electrically small antenna itself is an inefficient radiator, the antenna can instead be a probe that excites currents on the structure so the structure radiates rather than antenna acting as the radiator [11]. As a consequence, this should nominally aid in the radiation. Thus, this principle was used to see if there may be a better spot on the ground plane to place the electrically small AUT other than at the center of the ground plane, which was what was done in simulation.

The commercial computational electromagnetic solver FEKO was used because the software has a built-in characteristic mode analysis tool. This tool was used to determine the characteristic modes for the $8'x8'$ ground plane at each antenna's operating frequency. Results from the analysis showed that mode 1 for each of the frequencies possesses the highest modal weighting and was thus used for determining antenna placement. Figures 5.9-5.13 show the magnitude and direction of the first modal current for each antenna's operating frequnecy. Each modal current possesses a high medial intensity which conveniently points to optimal antenna placement at the center of the ground plane. Despite what the data shows, for sake of consistency, antenna orientation in the measurements for induced currents aren't lined up exactly with current modes displayed, but aligned with way they were simulated.

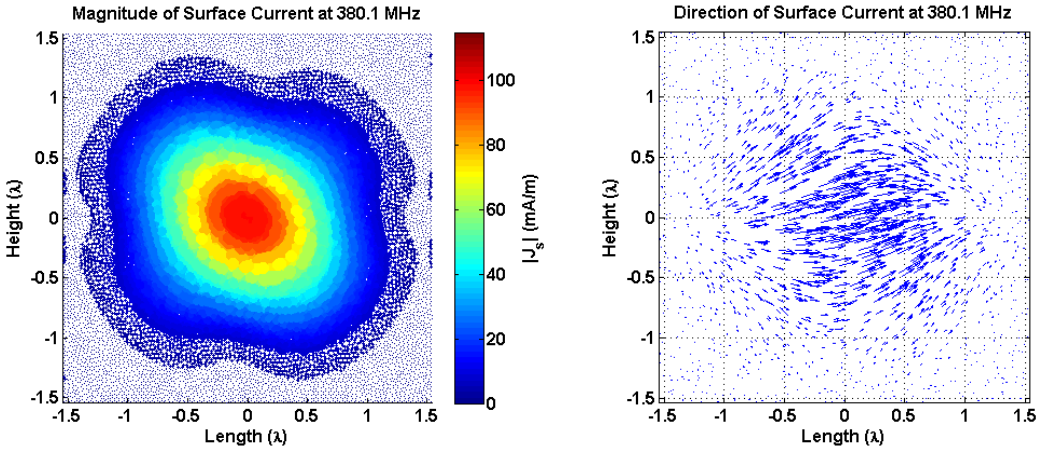
5.4 Measured Results

Scattering parameters of each antenna were obtained on a network analyzer to verify the operating frequency and impedance behavior of each antenna when compared to simulation. The comparisons between simulated and measured S_{11} are



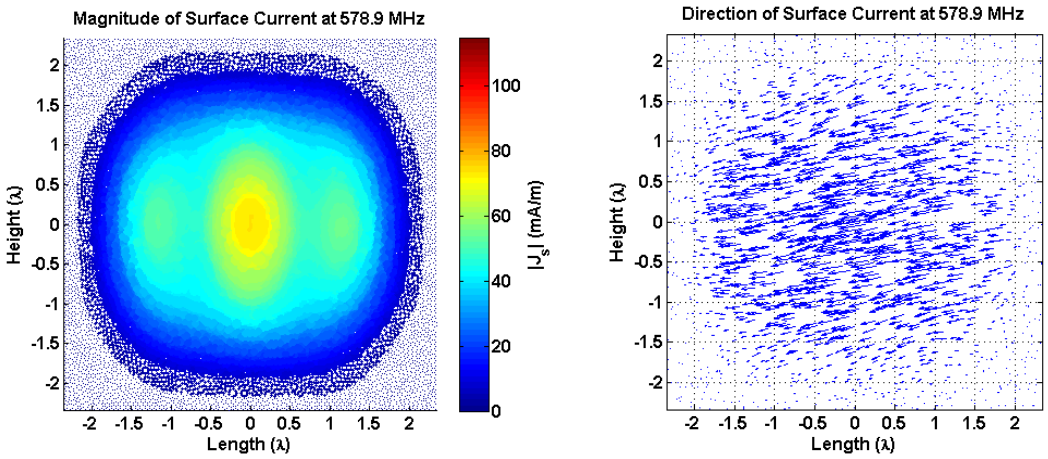
(a) (b)

Figure 5.9: (a) Magnitude and (b) direction of mode 1 surface currents on ground plane at 440.5 MHz, which corresponds to operating frequency of antenna containing triangular serration edge treatments. Length and height designated as electrical size of ground plane at operating frequency.



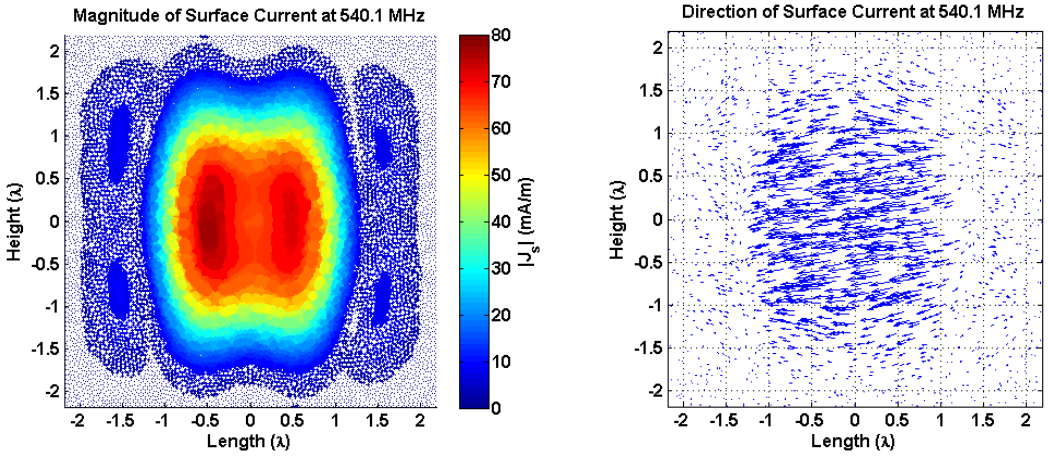
(a) (b)

Figure 5.10: (a) Magnitude and (b) direction of mode 1 surface currents on ground plane at 380.1 MHz, which corresponds to operating frequency of antenna containing ellipse serration edge treatments. Length and height designated as electrical size of ground plane at operating frequency.



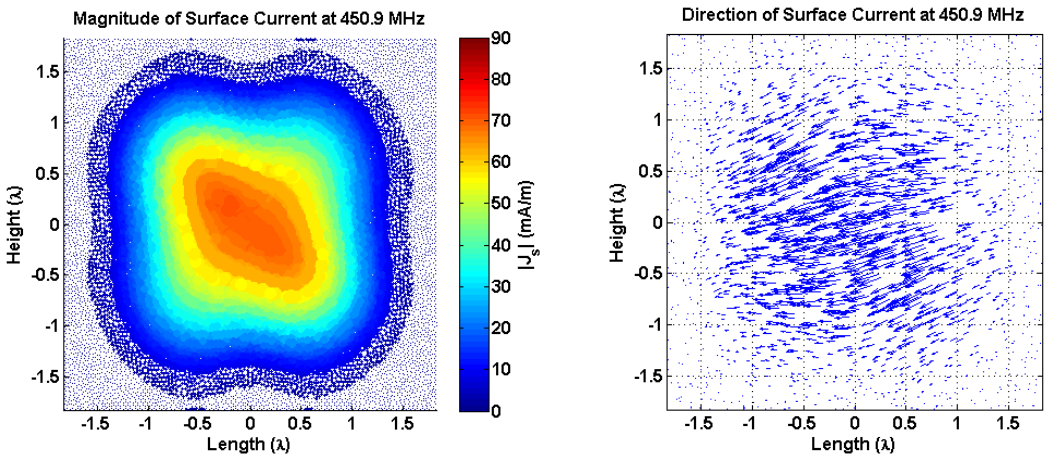
(a) (b)

Figure 5.11: (a) Magnitude and (b) direction of mode 1 surface currents on ground plane at 578.9 MHz, which corresponds to operating frequency of antenna containing curved serration edge treatments. Length and height designated as electrical size of ground plane at operating frequency.



(a) (b)

Figure 5.12: (a) Magnitude and (b) direction of mode 1 surface currents on ground plane at 540.1 MHz, which corresponds to operating frequency of antenna containing subtriangle serration edge treatments. Length and height designated as electrical size of ground plane at operating frequency.



(a) (b)

Figure 5.13: (a) Magnitude and (b) direction of mode 1 surface currents on ground plane at 450.9 MHz, which corresponds to operating frequency of antenna containing triangular aperture serration edge treatments. Length and height designated as electrical size of ground plane at operating frequency.

shown in Figures 5.14-5.18. There are some discrepancies in this measured data; particularly for the antennas containing the ellipse and curved serration edge treatment. This is likely due to fabrication tolerances of the lithography. The masks used to expose the correct design onto the photoresistive material for these two antenna's edge treatments were not professionally printed. The resolution of the mask images was low enough to not capture some of the finer features of these two edge treatments. For the ellipse serration, the point where two of the iterations converge to repeat the pattern wasn't captured properly. For the curved serration, the tips of the edge treatment converge to too fine of a point that also wasn't captured properly. These errors effectively change the physical dimensions of the edge treatments. This can account for some of the large frequency shifts that are observed in the measured data because the electrical size of the edge treatments are part of what determine the operating frequency of each antenna.

The setups for how measurements were obtained are pictured in Figures 5.6-

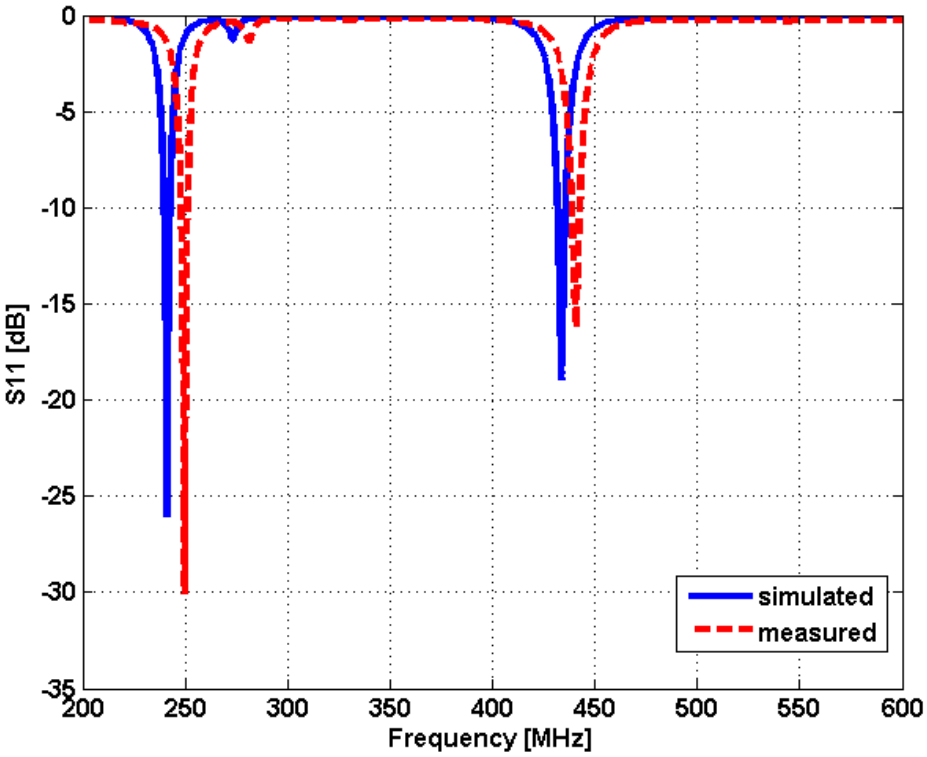


Figure 5.14: S_{11} measured vs simulated for the conductor-backed slot antenna containing the triangular serration edge treatment.

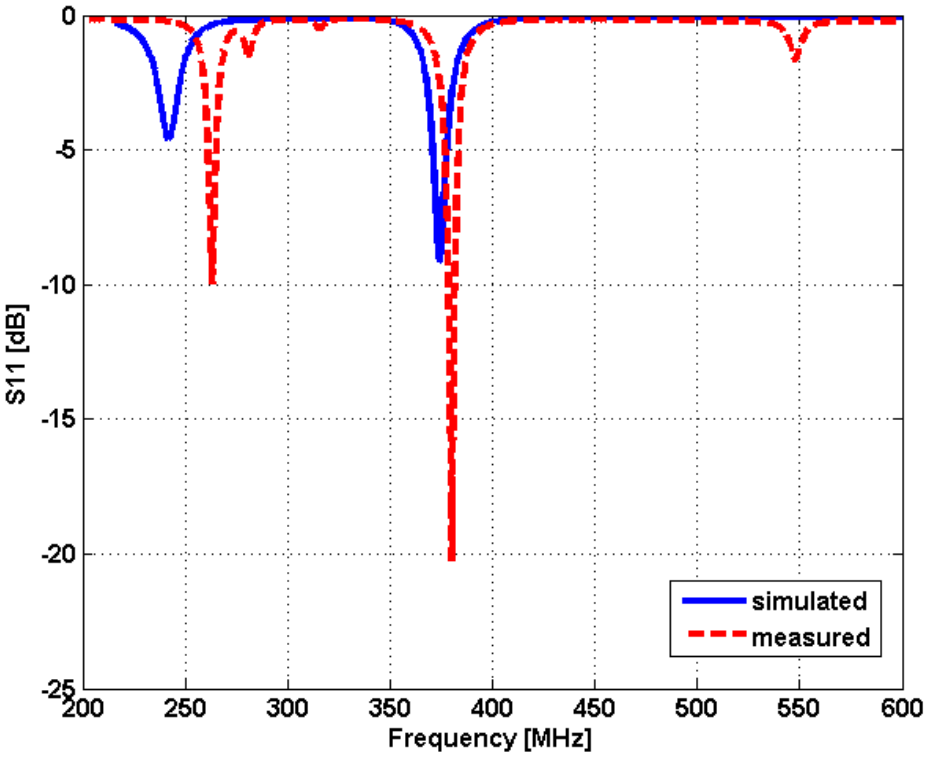


Figure 5.15: S_{11} measured vs simulated for the conductor-backed slot antenna containing the ellipse serration edge treatment.

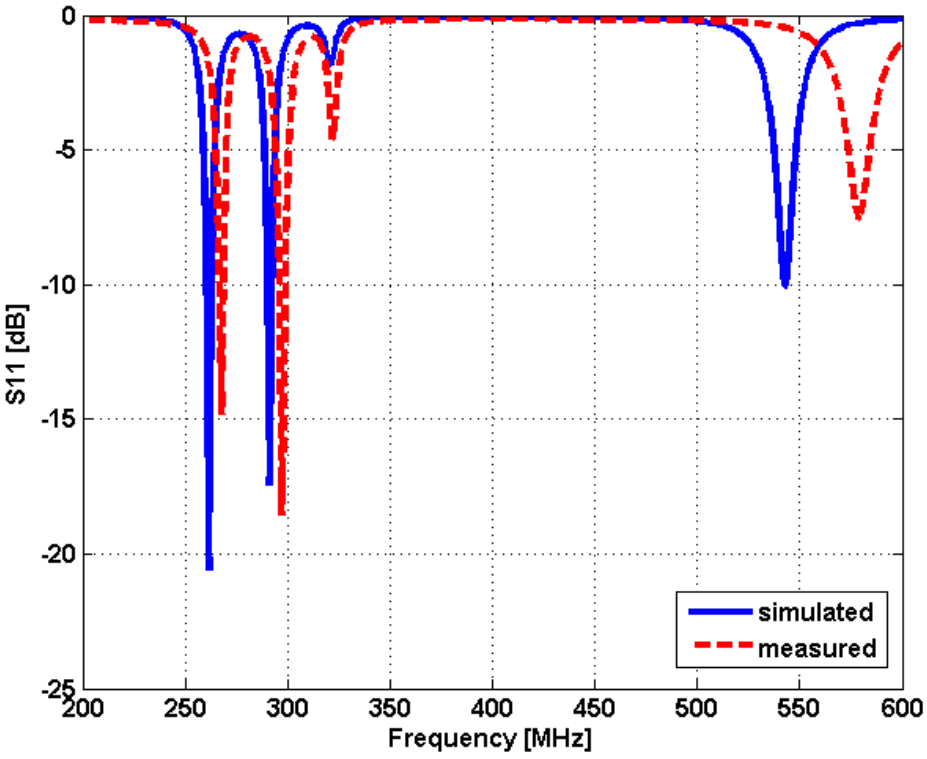


Figure 5.16: S_{11} measured vs simulated for the conductor-backed slot antenna containing the curved serration edge treatment.

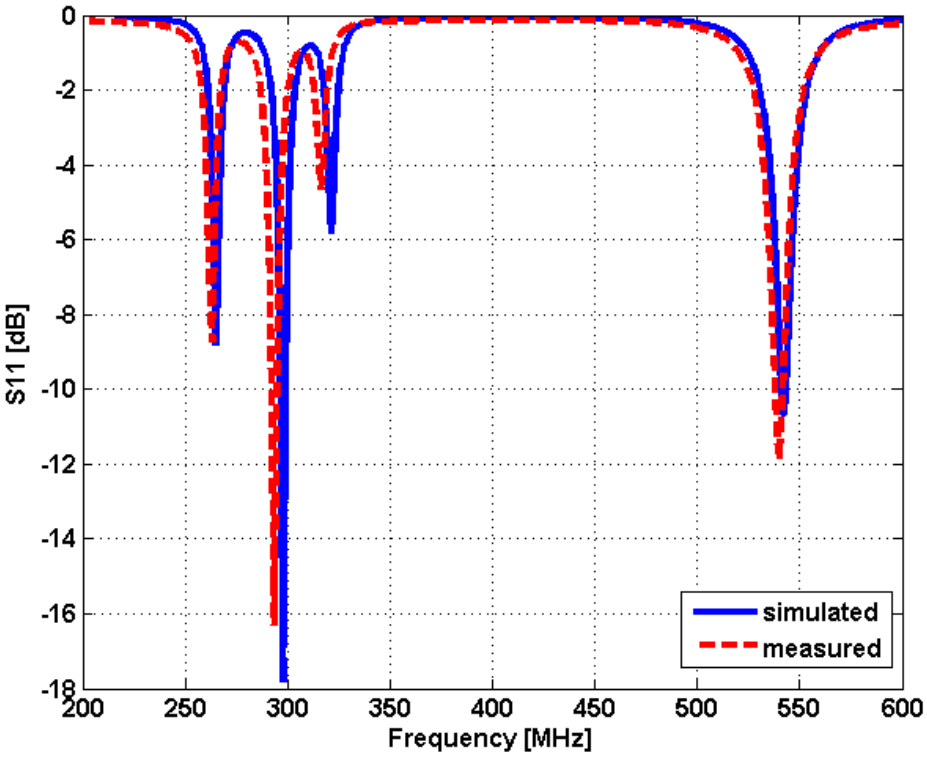


Figure 5.17: S_{11} measured vs simulated for the conductor-backed slot antenna containing the subtriangular serration edge treatment.

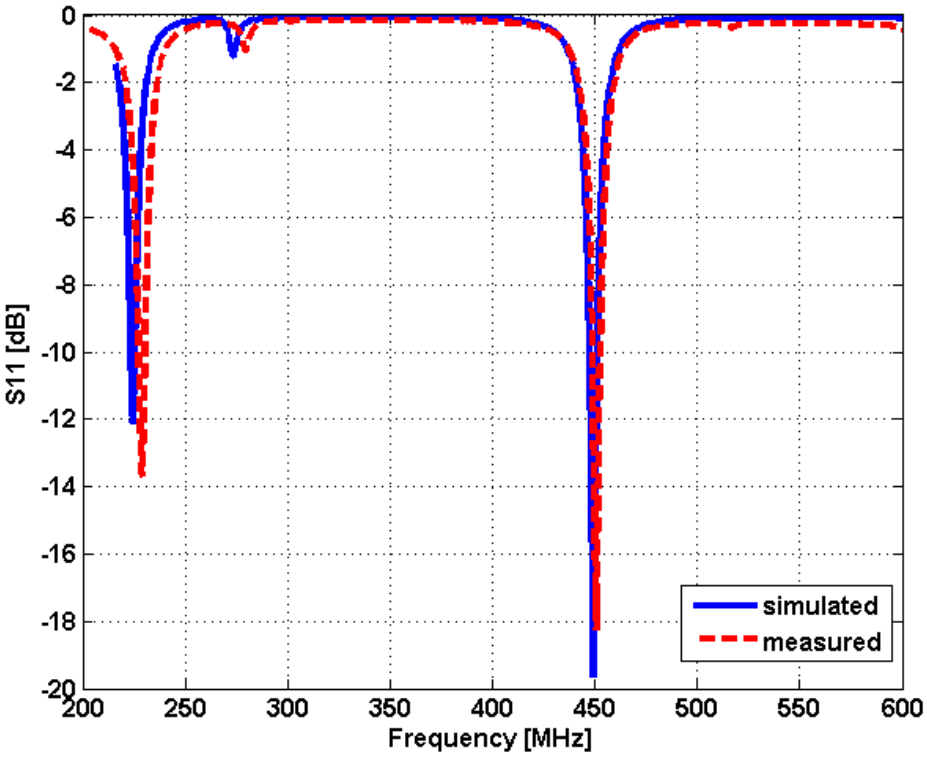
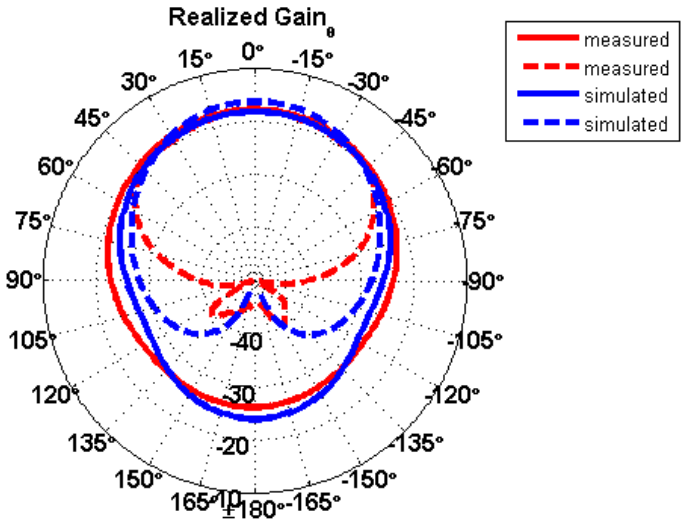
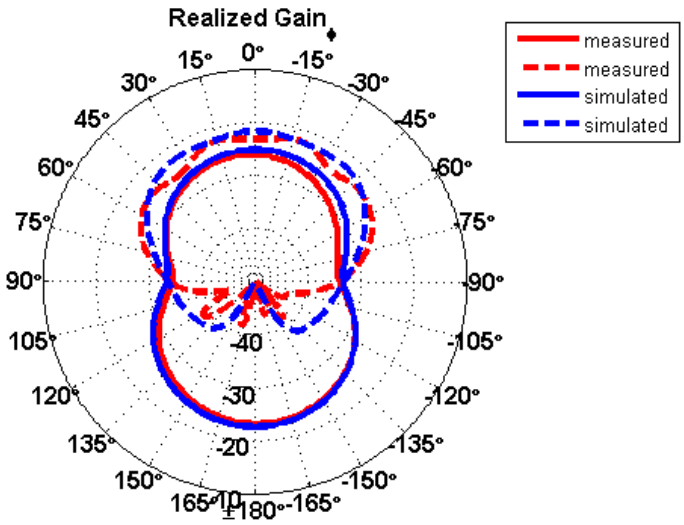


Figure 5.18: S_{11} measured vs simulated for the conductor-backed slot antenna containing the triangular aperture serration edge treatment.

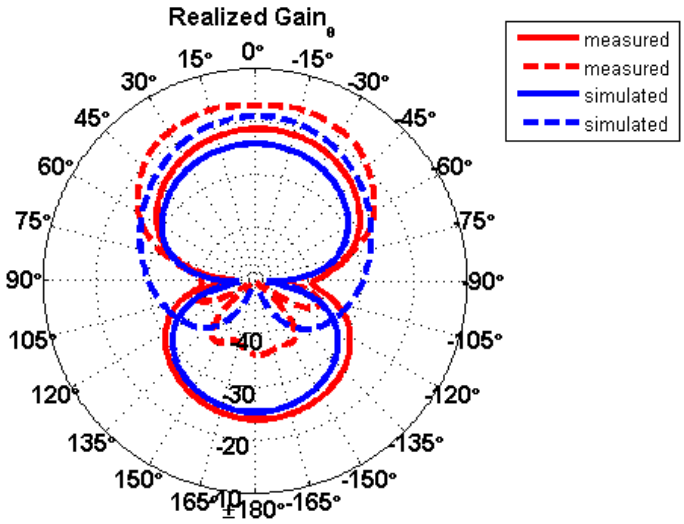


(a)

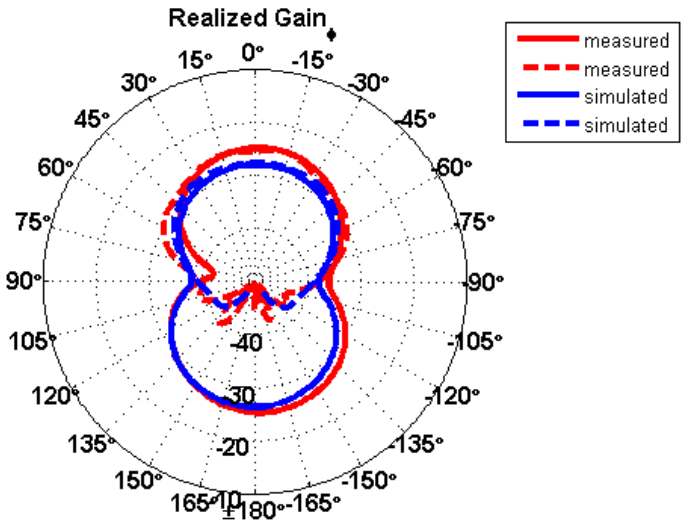


(b)

Figure 5.19: Measured vs simulated (a) realized Gain θ and (b) realized gain ϕ of antenna containing the triangular serration edge treatment. Solid lines correspond to antenna pattern without ground plane, while dashed lines correspond to antenna pattern mounted on ground plane.

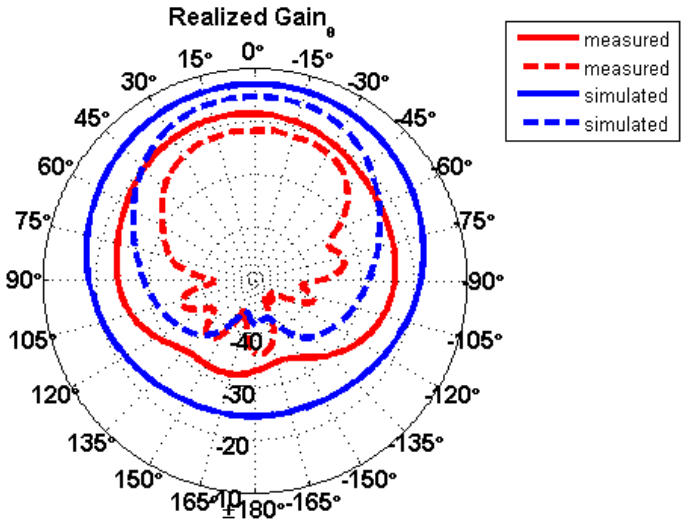


(a)

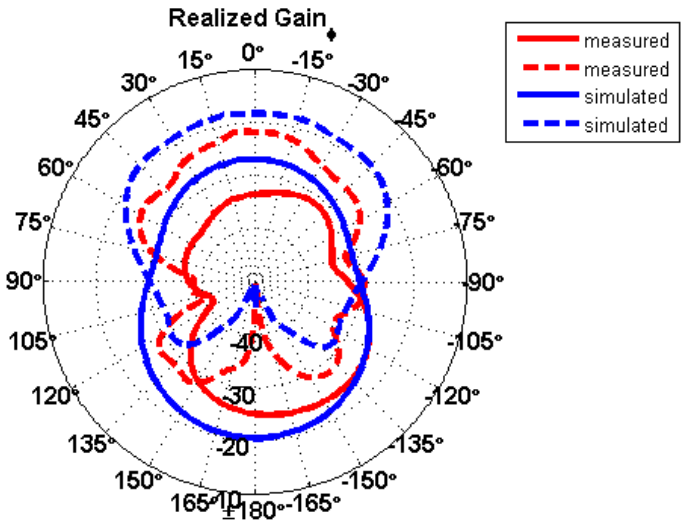


(b)

Figure 5.20: Measured vs simulated (a) realized Gain θ and (b) realized gain ϕ of antenna containing the ellipse serration edge treatment. Solid lines correspond to antenna pattern without ground plane, while dashed lines correspond to antenna pattern mounted on ground plane.

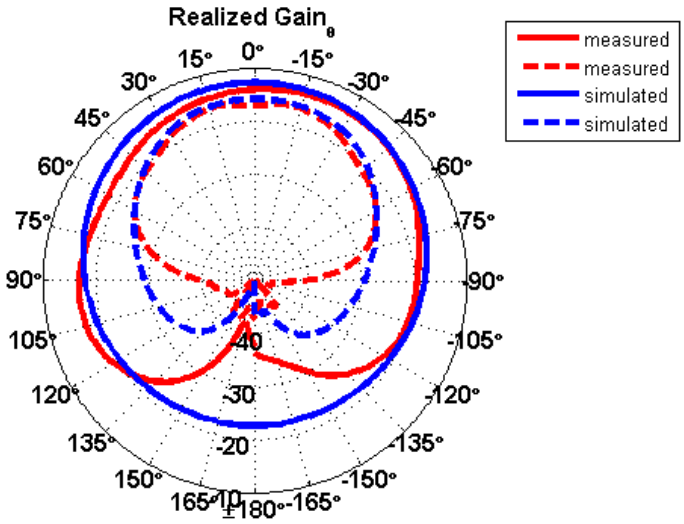


(a)

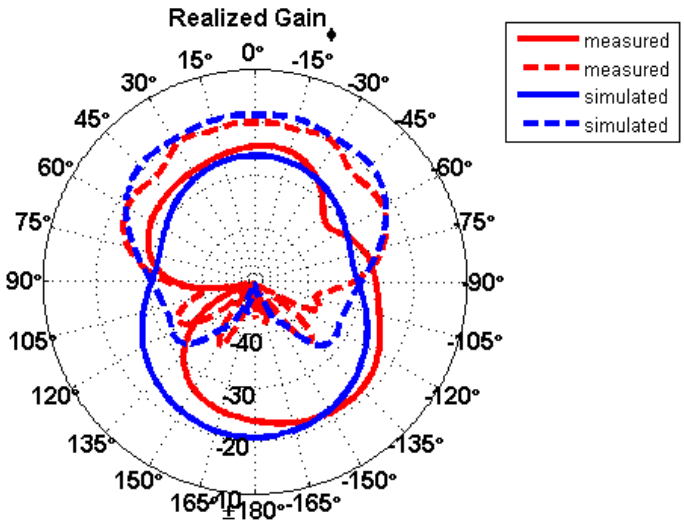


(b)

Figure 5.21: Measured vs simulated (a) realized Gain θ and (b) realized gain ϕ of antenna containing the curved serration edge treatment. Solid lines correspond to antenna pattern without ground plane, while dashed lines correspond to antenna pattern mounted on ground plane.

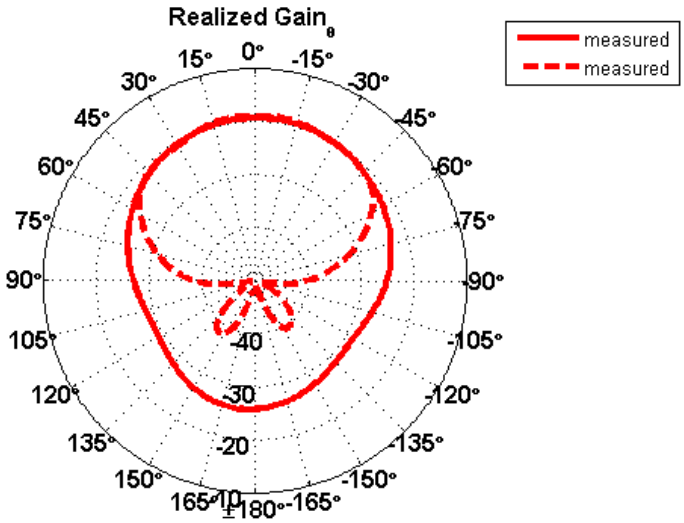


(a)

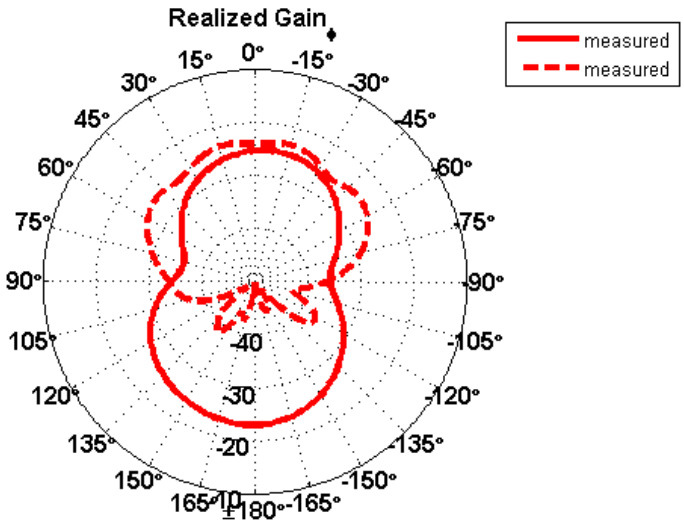


(b)

Figure 5.22: Measured vs simulated (a) realized Gain θ and (b) realized gain ϕ of antenna containing the subtriangular serration edge treatment. Solid lines correspond to antenna pattern without ground plane, while dashed lines correspond to antenna pattern mounted on ground plane.



(a)



(b)

Figure 5.23: Measured vs simulated (a) realized Gain θ and (b) realized gain ϕ of antenna containing the triangular aperture serration edge treatment. Solid lines correspond to antenna pattern without ground plane, while dashed lines correspond to antenna pattern mounted on ground plane.

5.8. The calibration dipole was used to extract accurate realized gain from the AUTs. Each dipole is first measured across a frequency band surrounding the operating frequency. The resulting pattern from each antenna with the largest gain is designated to have the maximum gain that is possible for a half-wave dipole. This value is subtracted from 2.15 dB, yielding a delta value that is added to subsequent antenna measurements. Next, each antenna is measured without the ground plane, adding the delta value afterwards. Then, each antenna is measured on the ground plane, adding the delta value afterwards. Figures 5.19-5.23 show the resulting realized gain patterns of the antennas both off and on the ground plane compared to patterns obtained from HFSS simulations. Only the theta and phi polarization (co-pol and cross pol) measurements for azimuth cut plane have been obtained because of the limited measurement capabilities available for the chamber.

The overall trends when comparing the simulated data to the measured data agree reasonably well. Discrepancies in the ground plane measurements, particularly for the back-plane radiation can be accounted from the different physical sizes of the simulated versus the constructed ground plane. The different physical sizes means that diffraction at the edges of the ground plane occurs at a different electrical sizes. Additionally, deviations in the magnitude of simulated versus measured data follow the trends for how much the fabrication tolerances shift the operating frequency of an antenna. This can be observed for the antenna containing the curved serration edge treatment where the measured data deviates by an amount that is consistent with the amount the operating frequency gets shifted by and the difference in magnitude for the impedance match.

Tables 5.1 and 5.2 provide the broadside realized gain for each antennas' measured and simulated co-pol and cross pol patterns. The triangular serration edge treatment starts out at a higher gain at co-pol, but experiences minimal increase in

	Truncated GP		Larger GP	
Edge Treatment	Sim. (dB)	Meas. (dB)	Sim. (dB)	Meas. (dB)
Triangular	-18.04	-17.60	-16.11	-17.83
Ellipse	-24.03	-21.26	-18.84	-16.81
Curved	-12.82	-18.37	-15.18	-21.62
Subtriangular	-12.49	-13.81	-15.59	-16.74
Apertures	N/A	-19.17	N/A	-18.79

Table 5.1: Measured and simulated broadside realized gain for each antenna when containing truncated conductor backing and when placed on larger ground plane. Data shown for co-pol (θ) patterns.

	Truncated GP		Larger GP	
Edge Treatment	Sim. (dB)	Meas. (dB)	Sim. (dB)	Meas. (dB)
Triangular	-24.99	-25.89	-21.47	-23.03
Ellipse	-27.79	-24.67	-27.46	-25.27
Curved	-26.76	-33.39	-18.17	-21.69
Subtriangular	-26.12	-24.33	-18.37	-19.82
Apertures	N/A	-25.16	N/A	-23.90

Table 5.2: Measured and simulated broadside realized gain for each antenna when containing truncated conductor backing and when placed on larger ground plane. Data shown for cross pol (ϕ) patterns.

gain when placed on a larger ground plane; at cross pol, this antenna starts out at a lower gain, but has a greater gain increase when placed on a larger ground plane. The gain data of the antennas containing the curved serration and subtriangle serration edge treatments show that increasing the electrical size of both the antenna and ground plane decreases the gain when antenna placed over the ground plane This could also depend on direction and magnitude of induced currents on the ground plane, meaning a different orientation at a different electrical size could yield better results. The antenna containing the ellipse serration edge treatment is the only antenna that experiences a gain increase at co-pol when placed on the larger ground plane, and also possesses the greatest difference in change in magnitude when com-

pared to the truncated backing case. For the antenna containing the aperture edge treatment, there is no appreciable radiation enhancement present when compared to the edge treatment without the apertures. Thus, adding an aperture into the edge treatment is not necessarily a sound technique for coupling into a ground plane, even though it might be a useful technique for other purposes. Otherwise, each antenna radiates in a fundamentally different way when they are all oriented the same direction which the mechanism is not quite understood yet and is a basis for future work.

5.5 Conclusions

Measurements of the edge treatments, as being included as part of the system of the placement insensitive antenna, were obtained with the antenna containing a truncated conductor backing and when the antenna is placed on a larger ground plane in order to verify the theoretical results obtained from simulations. Additionally, characteristic mode theory was used to determine optimal antenna placement on the ground plane according to each antenna's operating frequency. Although the placement strategy indicated that induced currents are medial, which does not line up with the direction that the antenna induced currents in simulation, the antenna placements were consistent with orientations presented in the simulations. Future work will involve orienting the antennas so induced currents line up with modal currents.

It was determined that electrical size and antenna placement/orientation are strong factors that determine antenna radiation behavior and how much induced currents will contribute to the radiation mechanism. The exact coupling mechanism, however, has yet to be determined and is thus a subject for future work.

Chapter 6

Conclusions/Future Work

6.1 Conclusions

Edge treatments on a parallel plate waveguide have been shown to be able to match the impedance of the waveguide to the impedance of freespace, allowing a greater power transfer from the source to radiated fields. Alternate edge treatment designs were investigated and viability for replacement of the triangular serration edge treatment on the placement insensitive antenna with a different edge treatment was examined. The guidelines of which antenna edge treatment to choose is highly dependent on the type of application that the antenna is to be used in. Using a half-circle edge treatment or a variation of it appears to be the best candidate if more broadband operation at smaller electrical sizes is desired. Complex coupling environments from higher order modes for the other edge treatments at larger electrical sizes present multi-band impedance matches of narrow bandwidth. Inclusion of an aperture shows to promote more constant or uniform radiation behavior across frequency. The operation of each edge treatment depends on numerous factors and exact characterization is difficult due to the excitation of higher order modes in the structures. With the results obtained and insights gathered, however, we can approach the edge treatment design process more strategically. Additionally, the edge

treatments investigated in this thesis don't have to be the exact edge treatment used in the design process. We can look at their individual properties to determine a potentially newer design that contains a combination of each of the edge treatment types.

The disconnected aperture arm, due to its most impressive impedance matching ability, was investigated as a viable edge treatment design on its own. Findings show that the disconnected arm is a microstrip resonator acting more like a transmission line impedance matching element than an effective radiator itself. The disconnected arm, however, may be useful to implement along with an actual edge treatment design that shows favorable performance. A transmission line model was derived to characterize the impedance behavior of the disconnected aperture arm structure, but is not accurate at larger electrical sizes for the structure due to higher order modes and other parasitics and coupling effects that have not been accounted for.

Edge treatments were investigated as a viable option for coupling energy into a ground plane so the ground plane can either aid in the radiation or become the radiator itself. Edge treatments can induce currents onto a ground plane, but the performance is highly dependent on the edge treatment type and electrical size of the edge treatment and ground plane present. Edge treatment behavior also changes from when it only contains the truncated conductor backing to when it is to radiate out onto an electrically larger ground plane. Thus, careful consideration must be applied in determining whether a specific edge treatment type is the most viable option for a scenario because its behavior can be much different than what is expected. It is possible that an alternative edge treatment type not investigated in this thesis may outperform the ones investigated if all the best features of each edge treatment are combined into a new type of edge treatment. The placement insensitive antenna, as a viable option for an electrically small probe to induce currents on

a ground plane, was examined. It was shown that the type of edge treatment present and its electrical size in the antenna design has an effect on the overall performance of the antenna when it is placed over a large ground plane.

6.2 Future Work

Future work will look at potential additional edge treatment types that may perform better than the ones currently investigated. Work will also be done to further refine the transmission line model of the disconnected aperture arm structure so all electromagnetic effects are accounted for. Determining the exact coupling mechanisms of the edge treatments into a ground plane still needs to be completed because it will provide additional insight into what edge treatment may work best. Additional placement insensitive antenna orientations and positions on the larger ground plane will be investigated. particularly in the case where the induced currents of the antennas line up with the modal currents of the ground plane.

References

[1] J. Ruyle, "Small, dual band, placement insensitive antennas", PhD thesis, University of Illinois at Urbana-Champaign, 2011.

[2] C. Balanis and Y.-B. Cheng, "Antenna radiation modeling for microwave landing system", *IEEE Transactions on Antennas and Propagation*, vol. 24, no. 4, pp. 490–497, Jul. 1976.

[3] J. Calusdian, "Radiation patterns of antennas installed on aircraft", Master's thesis, Naval Postgraduate School, Monterey, CA, Monterey, CA, Dec. 1998.

[4] W. D. B. E L Pelton Nan Wang, "Near field pattern analysis for aperture or monopole antennas mounted on an aircraft in the principal planes", Ohio State Univ Columbus Electroscience Lab, Tech. Rep., Jan. 1978.

[5] W. D. Burnside, "Analysis of on-aircraft antenna patterns", Ohio State Univ Columbus Electroscience Lab, Tech. Rep., Apr. 1974.

[6] R. E. Koehler, "Modeling uhf antenna coupling on aircraft", Master's thesis, Naval Postgraduate School, Monterey, CA, Monterey, CA, Mar. 1975.

[7] R. Garbacz and R. Turpin, "A generalized expansion for radiated and scattered fields", *IEEE Transactions on Antennas and Propagation*, vol. 19, no. 3, pp. 348–358, May 1971.

[8] R. Harrington and J. Mautz, "Theory of characteristic modes for conducting bodies", *IEEE Transactions on Antennas and Propagation*, vol. 19, no. 5, pp. 622–628, Sep. 1971.

[9] ——, "Computation of characteristic modes for conducting bodies", *IEEE Transactions on Antennas and Propagation*, vol. 19, no. 5, pp. 629–639, Sep. 1971.

[10] Y. Chen and C. F. Wang, "Synthesis of platform integrated antennas for reconfigurable radiation patterns using the theory of characteristic modes", in *ISAPE2012*, Oct. 2012, pp. 281–285.

[11] E. Newman, "Small antenna location synthesis using characteristic modes", *IEEE Transactions on Antennas and Propagation*, vol. 27, no. 4, pp. 530–531, Jul. 1979.

[12] R. G. I. Bahl and M. Bozzi, *Microstrip Lines and Slotlines*, 3rd ed. 685 Canton Street, Norwood, MA 02062: Artech House, 2013.

[13] R. Garg and I. Bahl, "Microstrip discontinuities", *International Journal of Electronics Theoretical and Experimental*, vol. 45, no. 1, pp. 81–87, 1978.

[14] J. E. R. A. M. H. K. A. Lietuvninkas, *Electrically small antenna design guide*, Univ. of Oklahoma Dept. of Elec. and Comp. Engr., 2015.

[15] D. Pozar, *Microwave Engineering*, 4th ed. Hoboken, NJ: John Wiley & Sons, 2012.

[16] C. Balanis, *Antenna Theory: Analysis and Design*, 3rd ed. Hoboken, NJ: John Wiley & Sons, 2005.

[17] ——, *Advanced Engineering Electromagnetics*, 2nd ed. Hoboken, NJ: John Wiley & Sons, 2012.